ACS Sustainable Chemistry & Engineering

pubs.acs.org/journal/ascecg

Research Article

Amphiphilic Copolymer Thin Films with Short Fluoroalkyl Side Chains for Antibiofilm Properties at the Solid−Liquid−Air Interface

Alexandra Khlyustova, Mia Kirsch, and Rong Yang*

Cite This: https://doi.org/10.1021/acssuschemeng.2c03933

Read Online

ACCESS | Metrics & More | Article Recommendations | Supporting Information

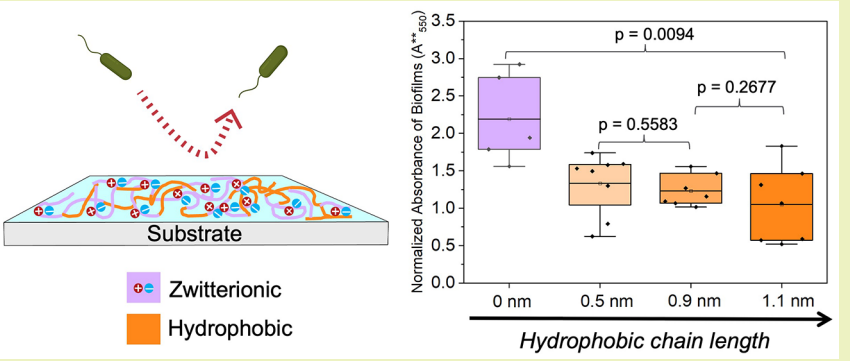

ABSTRACT: Biofouling is a critical problem that limits numerous technologies including water desalination and marine transportation. The existing solutions, such as copper-based paint to mitigate ship hull fouling, are known to harm aquatic species. Although hydrophilic and zwitterionic materials have demonstrated great promise in resisting the formation of biofilms, they demonstrated limited effectiveness at the solid−liquid−air interface, the location most prone to biofilm formation by motile bacteria. While an amphiphilic copolymer comprising a statistical mixture of zwitterionic and fluorinated units exhibited excellent antifouling performance at the triple interface, the long-fluorinated side chain raises concerns regarding bioaccumulation. Here, two amphiphilic copolymers, each made of a pyridinium-based zwitterionic and hydrophobic repeat units with a short fluorinated chain (1*H*,1*H*,2*H*,2*H*-perfluorooctyl and 2,2,3,4,4,4-hexafluorobutyl groups), were synthesized using *initiated* chemical vapor deposition. Fineman−Ross analysis demonstrated the formation of random copolymers with a preference for 4-vinylpyridine incorporation. The antibiofilm performance remained good for both hydrophobic chains: amphiphilic copolymers outperformed pure zwitterionic chemistry by 43.8 and 39.3%, as demonstrated using *Pseudomonas aeruginosa* that forms biofilms at the triple interface. The amphiphilic coatings reported here can be used to prevent biofilm formation at the triple interface in marine transportation, food manufacturing, and medical devices, while avoiding the environmental concerns related to perfluoroalkyl substances.

KEYWORDS: *initiated chemical vapor deposition, amphiphilic coatings, antibiofilm, fluorinated polymer, biofilm*

INTRODUCTION

Biofouling is the accumulation of organic matter and (micro)organisms on a submerged surface. Its detrimental effects are manifested in virtually all aspects of society. For example, biofouling leads to long-standing problems of severe clogging of pipelines and filters,[1] secondary infections due to contamination of medical devices,[2,3] reduction of water quality in water purification systems,[4] and deterioration of fuel efficiency in marine transportation.[5] To resist biofouling, general strategies explored thus far include incorporation and sustained release of biocides[6] and surface modification with antifouling coatings to repel the adhesion.[7,8]

Biocides are commonly antimicrobial agents.[9,10] One of the first antifouling paints contained liquid tributyltin, which maintained 0% fouling for up to 49 months.[11] However, tributyltin has long been prohibited due to its strong ecotoxicity, which was believed to cause damage to the habitats of prosobranch species in Europe.[12] The current mainstay antifouling ship hull paint contains copper/zinc, which nevertheless has recently been shown to be harmful to aquatic life such as mussels and macroalga.[13] Furthermore, the effectiveness of biocide-based antifouling strategies has been declining steadily due to the rapid development of antimicrobial resistance. Biofilms of environmental bacteria formed on copper- and/or zinc-containing paints in natural aquatics have been shown to develop resistance to metals, as

Received: July 1, 2022
Revised: November 3, 2022
Published: November 18, 2022

well as antibiotics (like cefotaxime, tetracycline, and kanamycin) via a resistance development mechanism, namely co-selection.[14−19]

To overcome the ecotoxicity issues of biocide-based antifouling strategies, antifouling and fouling-release coatings have been developed. Hydrophilic antifouling coatings form a strong hydration layer via hydrogen bonding and/or dipole−dipole interactions with water molecules to create an enthalpic barrier to surface adhesion and thereby prevent fouling.[20] Furthermore, certain polymer brush-based antifouling coatings, such as poly(ethylene oxide) [PEO] brushes,[21] have been hypothesized to repel foulants via entropic effects (in addition to the aforementioned enthalpic penalty), that is, the entropy-based resistance to polymer chain compression that could result from the adhesion of foulants.[22] In the past decade, zwitterionic polymers, a class of hydrophilic materials with extremely strong hydration and hence excellent antifouling performance (due to the electrostatic interactions between their charged groups and induced dipole in water molecules), have been the focus of many antifouling studies.[23,24]

Even though zwitterionic coatings repel incoming bacteria at the solid−liquid interface, they have been demonstrated to be less effective at the solid−liquid−air interface, the location most prone to biofilm formation by motile gram-negative (e.g., *Pseudomonas aeruginosa*)[25,26] and gram-positive (e.g., *Bacillus cereus*)[27] bacteria. This interface provides a prolific environment for the formation of biofilms from a variety of environmental bacteria such as *Salmonella enterica*,[28] *Pseudomonas fluorescens*,[29] and *Acinetobacter*,[30] among others.[31−34] The solid−liquid−air interface is becoming a critical problem for biofouling prevention in natural aquatics because the amount of biofilm formation at this interface greatly outnumbers that in submerged systems.[35] That preferential formation of biofilms at the solid−liquid−air interface is driven by the easy access to nutrients and oxygen at the surface of a liquid layer, which has been found in other eukaryotic fouling species,[35] such as algae[36] and barnacle cyprids, the latter of which are known to swim close to the air−water and water−solid interfaces and settle there.[37] To address the challenge of biofouling at the solid−liquid−air interface, we recently developed an amphiphilic copolymer consisting of a statistical mixture of pyridinium-based zwitterionic and 1*H*,1*H*,2*H*,2*H*-perfluorodecyl acrylate (PFDA) repeat units using an all-dry synthesis technique, namely *initiated* chemical vapor deposition (iCVD). The amphiphilic copolymer outperformed conventional zwitterionic chemistry by further reducing biofilm formation at the triple interface by 61%.[38] While amphiphilic coatings have also been reported to reduce biofouling at the solid−liquid interface in past studies,[39] its effectiveness at the triple interface stands out and makes the amphiphilic coatings an attractive candidate for biofouling prevention across the water-contacting surfaces of a ship hull. The existing antifouling solutions (such as copper- and/or zinc-containing paints) may not deliver these benefits.[40]

Despite the outstanding antifouling performance, the PFDA repeat unit in that amphiphilic copolymer could undergo hydrolysis to produce C_8 perfluoroalkyl substances (PFAS), which have been under increasing scrutiny due to evidence of environmental persistency, long-range transport, bioaccumulation potential, and/or toxicity.[41] Shorter-chain PFAS (i.e., with <7 fluorinated carbons) have demonstrated a lower tendency to adsorb/absorb into biosolid matrices[42] and thus have the potential to replace their long-chain counterparts to reduce the environmental impact. Nevertheless, polymers with shorter fluorinated side chains may be less hydrophobic, which could lead to reduced antifouling effectiveness in the context of amphiphilic materials design. That trade-off remains elusive in the existing literature, which hinders the development of antifouling coatings with a minimal environmental impact.

To address that knowledge gap, we systematically investigated the antifouling performance of amphiphilic copolymers made with varying lengths of fluorocarbon side chains, with an emphasis on monomers with <7 fluorinated carbons. The reactivity during copolymerization with 4-vinylpyridine (4VP, the precursor for the zwitterionic moieties in the final amphiphilic copolymer) and the resulting domain size of the amphiphilic heterogeneities were analyzed in detail in the context of their resistance to biofilm formation at the triple interface. Specifically, 1*H*,1*H*,2*H*,2*H*-perfluorooctyl acrylate (PFOA, with six fluorocarbons in the side chain) and 2,2,3,4,4,4-hexafluorobutyl acrylate (HFBA, with three fluorocarbons in the side chain) were chosen based on the evidence that the degradation products of their fluorocarbon side chains have minimal bioaccumulation in the liver of rats compared to that of perfluorooctanesulfonic acid.[43] While recent evidence hinted that PFOA could cause accumulation in serum,[43] HFBA (n = 3) has demonstrated low bioaccumulation potential and low toxicity in past reports.[44] PFAS with n = 3 have been shown to lead to undetectable cytotoxicity when tested on human mesenchymal stem cells for over 7 days of incubation[45] and to cause the lowest level of bioaccumulation (among a selection of six fluorinated compounds) in the serum of rats over 10 days.[43] The cumulative amount was merely one-third that of substances with seven fluorocarbons and thus deemed safer for long-term applications.[43] Even when injected with PFAS with n = 3, test animals (rats in this case) only experienced mild toxicity, as manifested by a slight increase in the weight of their liver. Additionally, the toxicity of PFAS has been evaluated using a zebrafish liver cell line, and PFAS with n = 3 demonstrated the lowest cytotoxicity among 11 compounds with varying numbers of fluorocarbons.[46] Specifically, with the introduction of 100 and 250 ppm of PFAS (n = 3), the cell viabilities were 98 ± 16% and ∼75%, respectively, after 96 h of incubation,[47] indicating that HFBA (n = 3) has low bioaccumulation potential and low toxicity.

iCVD has been proven to be a versatile tool to produce amphiphilic thin films with nanometer-scale heterogeneities (1−2 nm^2) by avoiding surface-tension-driven instability[48] and microphase separation; it thus compares favorably to solution-based synthetic methods for making nanoscale amphiphilic surfaces with molecular heterogeneities.[49] As such, it has been used to copolymerize 2-hydroxyethyl methacrylate (HEMA) and PFDA, yielding an amphiphilic copolymer that was antifouling against *Escherichia coli*.[50,51]

Using the iCVD technique, poly(4-vinylpyridine-*co*-1*H*,1*H*,2*H*,2*H*-perfluorooctyl acrylate) [P4VP-*co*-PFOA] and poly(4-vinylpyridine-*co*-2,2,3,4,4,4-hexafluorobutyl acrylate) [P4VP-*co*-HFBA] copolymers were synthesized at various compositions. Fineman−Ross analysis proved the formation of statistical copolymers without microphase separation with domain size that is equivalent to monomer length, which was corroborated experimentally using atomic force microscopy (AFM). *Pseudomonas aeruginosa* (PAO1) was used as a model strain to test the antibiofilm performance of the amphiphilic copolymers, which is a prolific biofilm former at the triple interface in nutrient-rich laboratory media like lysogeny broth

https://doi.org/10.1021/acssuschemeng.2c03933
ACS Sustainable Chem. Eng. XXXX, XXX, XXX−XXX

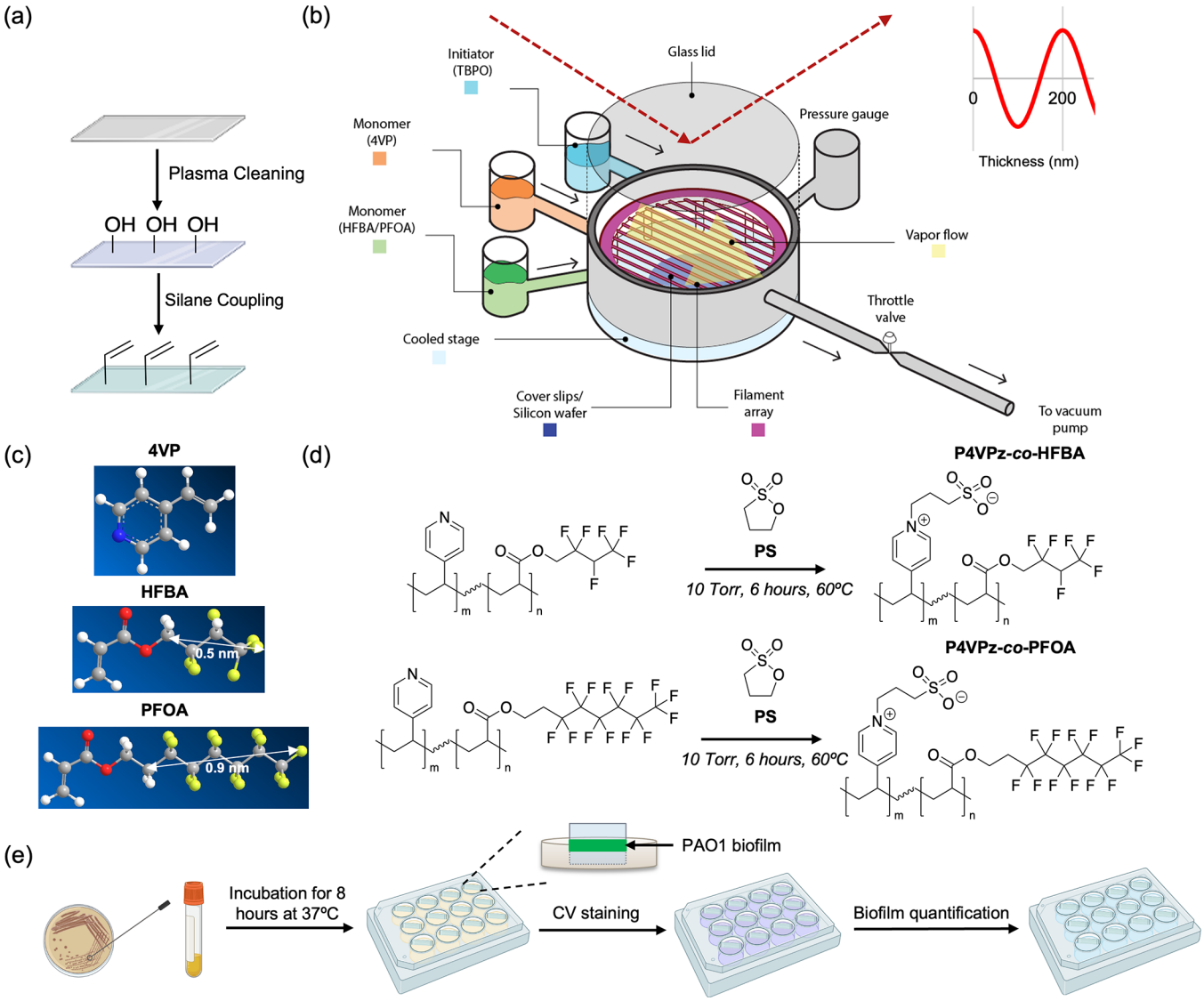

Figure 1. (a) Schematic of the substrate preparation steps. (b) Schematic illustration of the iCVD reactor. Reproduced with permission from ref. 75. Copyright 2021 Frontiers. (c) 3D structures of 4VP, HFBA, and PFOA monomers with respective perfluorinated side chain lengths. (d) Reaction of 1,3-propane sultone with P4VP-*co*-HFBA and P4VP-*co*-PFOA copolymers to produce their versions with zwitterionic moieties. (e) Scheme of the experimental steps for testing bacterial adhesion. (a) and (e) were prepared using BioRender.

(LB).[38] While this choice is motivated by our goal to assess and compare the performance of the statistical amphiphilic copolymers, it is important to note that PAO1 is not an ideal strain to assess biofilm formation under natural environments like seawater.[52] Against PAO1 biofilms, the amphiphilic copolymers with short, fluorinated chains demonstrated comparable effectiveness as their long-chain counterparts, pointing to their potential to be broadly adopted in the food processing industry, ship hull, water purification, medical implants, to mitigate biofilm formation without causing significant health and/or environmental detriments.

MATERIALS AND METHODS

Chemicals and Materials. The monomers 4VP (≥95%), HFBA (95%), divinylbenzene (DVB, 80%), and initiator *tert*-butyl peroxide (TBPO, 98%) were acquired from Sigma-Aldrich. The monomer PFOA (97%) was obtained from Synquest Laboratories. Trichlorovinylsilane (TCVS, 97%) and 1,3-propanesultone (PS, 98%) were acquired from Sigma-Aldrich. The 18 × 18 mm glass cover slips (12542A) were purchased from Fischer Scientific. The silicon (Si) wafer substrates were acquired from Pure Wafer. For biofilm attachment experiments, crystal violet (CV, Alfa Aesar), acetic acid (AA, 100%, Merck), and LB (240230, Difco) were used. All chemicals were used as purchased without further purification. A Milli-Q unit (Millipore) was used to produce deionized water with a resistivity of 18.2 MΩ-cm at 25 °C for all experiments.

Substrate Preparation. The schematic for substrate preparation is depicted in Figure 1a. Prior to deposition, glass cover slips and a Si wafer were cleaned in a PDC-001-HP plasma cleaner (Harrick Plasma) for 2−3 min at a pressure below 100 mTorr and a high RF setting of 45 W. After this treatment, the substrates were exposed to TCVS under vacuum for 5 min to chemically bond the iCVD copolymer thin film to the substrate to prevent film delamination.[53]

iCVD Synthesis. The scheme of the experimental setup for iCVD depositions is shown in Figure 1b with the respective monomer 3D structures of 4VP, HFBA, and PFOA in Figure 1c. The copolymers as well as their corresponding homopolymers were deposited in the custom-built reactor with a 2.5 cm thick glass lid to allow *in situ* laser interferometry (He−Ne laser, JDSU, USA) for visual observation and coating thickness control. The pressure was maintained at the specified set point by a throttle butterfly valve (MKS Instruments,

https://doi.org/10.1021/acssuschemeng.2c03933
ACS Sustainable Chem. Eng. XXXX, XXX, XXX−XXX

USA), and it was measured by a capacitance manometer (Baratron, MKS Instruments, USA). The stage temperature was set by an Accel 500 LC chiller (Thermo Fisher, USA) and measured by a type K thermocouple (Omega Engineering, USA). The TBPO initiator decomposition was enabled by the filament array, which consisted of copper/nickel wire (2.8 cm above the stage) that was resistively heated by a DC power supply (B&K Precision, USA). The filament temperature was also measured by a type K thermocouple. For P4VP-*co*-HFBA depositions, the deposition flow rates are summarized in Table 1. The reactor pressure was maintained at 1.1 Torr.[54] Both

Table 1. Flow Rates for P4VP-*co*-HFBA Depositions[a]

4VP flow rate (sccm)	HFBA flow rate (sccm)	TBPO flow rate (sccm)	argon flow rate (sccm)	f_{4VP} (%)
0.15	2.45	1.0	3.4	10.8
0.2	2.0	1.0	3.8	17.9
0.5	2.5	3.0	1.0	28.9
1.0	2.0	1.0	3.0	49.8
2.0	2.0	1.0	2.0	66.4
3.0	1.5	1.0	1.5	80.0

[a] f_{4VP} represents the 4VP monomer concentration (mole fraction) at the substrate surface.

monomers were fed into the reactor through needle valves (Swagelok, USA), and the monomer jar temperatures were maintained at 25 °C for HFBA and 50 °C for 4VP, respectively. The flow rate range for 4VP (vapor pressure of 1.68 Torr at 25 °C) was 0.1−3.0 sccm, while the HFBA (vapor pressure of 3.5 Torr at 25 °C) flow rate was 1.5−2.5 sccm. The initiator was kept at room temperature and delivered into the reactor at 1 sccm through the mass flow controller (MKS Instruments, USA). The total flow rate was kept constant at 7.0 ± 0.1 sccm to maintain a similar residence time in the reactor. The filament temperature was maintained at 250 °C, while the stage temperature was fixed at 27.1 ± 2.9 °C. The monomer feed gas fraction of 4VP (f_{4VP}) was calculated at the surface by correcting the monomer partial pressure of 4VP in the feed by its saturation vapor pressure (see Supporting Information).[55] Once the thickness of copolymer thin films reached 100 nm, the cover slips were flipped and coated with approximately 100 nm on the opposite side.

Similarly, Table 2 shows the summary of deposition flow rates for P4VP-*co*-PFOA. The reactor pressure was kept at 0.25 Torr to avoid

Table 2. Flow Rates for P4VP-*co*-PFOA Depositions

4VP flow rate (sccm)	PFOA flow rate (sccm)	TBPO flow rate (sccm)	argon flow rate (sccm)	f_{4VP} (%)
0.3	0.3	0.5	0.2	16.8
0.3	0.2	0.5	0.2	30.3
0.6	0.2	0.5	0	33.9
0.5	0.1	0.5	0.2	52.4

condensation due to the low vapor pressure of PFOA (0.332 Torr at 25 °C).[56] PFOA was heated to 60 °C and metered through a needle valve. The total flow rate was kept constant at 1.2 ± 0.1 sccm. The filament temperature was maintained at 250 °C, while the stage temperature was kept at 28.1 ± 1.1 °C. To compare the performance of amphiphilic thin films (P4VP-*co*-HFBA and P4VP-*co*-PFOA) to conventional zwitterionic coating, zwitterionic 4VP films crosslinked with DVB were synthesized (P4VPz) (See Supporting Information for deposition conditions).

Vapor-Phase Derivatization. The reaction schemes for the subsequent vapor-phase derivatization of P4VP-*co*-HFBA and P4VP-*co*-PFOA copolymers are shown in Figure 1d. After iCVD deposition, the coated substrates were exposed to PS vapor to make pyridinium-based sulfobetaine zwitterionic functional groups.[57] 1 g of PS was added to the crystallizing dish (VWR), while the specimens were fixed on the top of the dish. The dish was wrapped in aluminum foil and placed into a vacuum oven (VivTek, FVL-A30) with a medium level of vacuum (10 Torr) at 60 °C for 6 h.

Characterization. The thickness of the thin films on flat Si wafer substrates was measured by a J.A. Woollam Alpha-SE ellipsometer (Lincoln, NE) at incidence angles of 65°, 70°, and 75° using 190 wavelengths from 315 to 718 nm.[58] A Cauchy-Urbach model was used to fit the data and calculate the coating thickness and refractive index. A Bruker Vertex V80V (Billerica, MA) Fourier-transform infrared (FTIR) spectrometer with a cooled mercury cadmium telluride detector was used to determine the composition of thin films. The spectra were obtained from 450 to 4000 cm^{-1} with 4 cm^{-1} resolution and 128 total scans. The background spectrum of a Si wafer was subtracted from all samples, and the baseline was corrected using Origin Lab (Northampton, MA). Then, the spectra were normalized by the film thickness of each sample. X-ray photoelectron spectroscopy (XPS) was done using a Scienta Omicron ESCA 2SR (Uppsala, Sweden) under ultra-high operating pressure of 1×10^{-9} Torr. X-rays were generated from Al Kα at 300 W (15 kV; 20 mA) with an analysis spot size of 2 mm in diameter. A flood gun was used to neutralize nonconductive copolymer samples. Survey and high-resolution N(1s) and C(1s) scans were collected for all samples. The analysis of the spectra to determine film composition and correct background was performed with CasaXPS software. An Asylum MFP-3D (Goleta, CA) atomic force microscope was used to measure the surface roughness in AC air-tapping mode. At least two images at different locations were taken by scanning 5 × 5 μm regions at a frequency of 0.5 Hz. Dynamic contact angles, that is, advancing and receding contact angles, were measured with the sessile drop method by using a goniometer equipped with an automatic dispenser (Model 500, Rame-Hart). A droplet of 1 μL was deposited on the surface and increased up to 10 μL, and then, it was retracted. The advancing contact angle (θ_A) was recorded as the plateau angle during the increase in drop size, while the receding angle (θ_R) was the angle at which the angle plateaued while the volume was reduced from 10 to 3 μL.[59] At least three measurements were performed on each sample and averages were reported. The Bruker D8 powder diffractometer (Billerica, MA) was used to confirm the absence of crystallinity of the copolymers.

Calculation of Monomer Size and Perfluorinated Chain Length. Chem3D version 20.1.1 was used to develop a model for each monomer, and the distance between the two farthest points was measured to estimate the monomer size, and the distance between the farthest fluorine atom and nearest fluorine-free carbon was calculated to determine the length of the perfluorinated chain.

Biofilm Formation Experiments. The schematic of the main experimental steps to culture biofilm is shown in Figure 1e.[38] PAO1 strain of *P. aeruginosa* was used. A single colony of PAO1 was added to 5 mL of LB medium and incubated overnight until the OD_{600} reached 0.5−0.6. The absorbance was measured by a Tecan Infinite M1000 PRO. Then, this culture media was diluted 1:100 into fresh LB medium. A 12-well plate (3513, Corning) with attached coated cover slips was exposed to UV for disinfection for at least 30 min. 3 mL of the diluted culture media was added to each well along with two LB control wells. The lid with cover slips was placed on top of the well plate, such that samples stay vertical in the medium to ensure biofilm growth at the solid−liquid−air interface, and then incubated for 8 h at 37 °C. This 8-h incubation was selected because it allows *P. aeruginosa* biofilm to reach stage III of its lifecycle, leading to the formation of vertical and linear biofilms, the qualification of which is known to be reliable.[60,61] Similar conditions have been used in the past to assess the biofilm formation on amphiphilic copolymers.[38] After the incubation, the cover slips were washed with Milli-Q water and then submerged into 0.5% (w/v) CV solution for 15 min. The samples were dried overnight and then submerged into 33% (v/v) AA for 15 min to dissolve the stained biofilm. Finally, the OD_{550} was recorded for each sample as well as two control samples of AA for background correction.

https://doi.org/10.1021/acssuschemeng.2c03933
ACS Sustainable Chem. Eng. XXXX, XXX, XXX−XXX

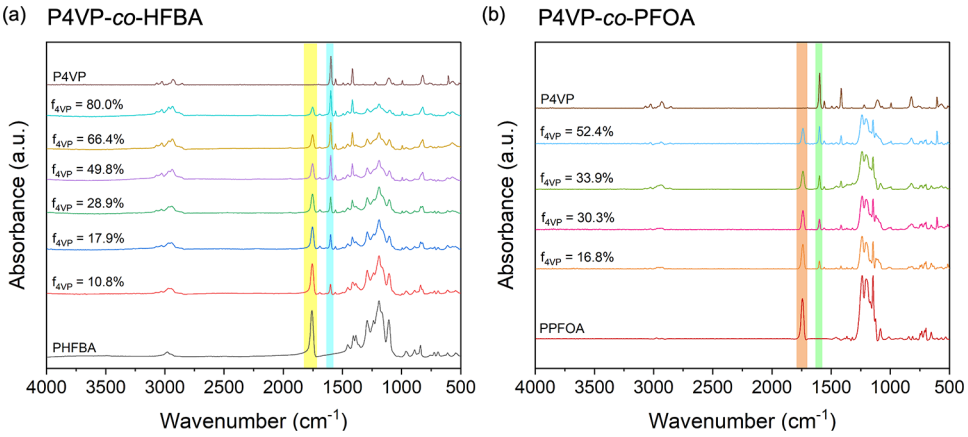

Figure 2. (a) FTIR of P4VP-*co*-HFBA copolymers with different 4VP gas fractions (f_{4VP}) and their corresponding homopolymers. The characteristic adsorption of HFBA is highlighted in yellow and corresponds to the C═O peak located at 1757 cm^{-1}. The characteristic adsorption of 4VP is highlighted with blue and corresponds to a peak due to the pyridine ring located at 1599 cm^{-1}. (b) FTIR of homopolymers of 4VP and PFOA, and their corresponding copolymers with various f_{4VP}. The characteristic adsorption of PFOA is highlighted in orange and corresponds to the C═O peak located at 1743 cm^{-1}. The characteristic adsorption of 4VP is highlighted with green and corresponds to the peak due to the pyridine ring located at 1599 cm^{-1}.

RESULTS AND DISCUSSION

Synthesis of the Amphiphilic Copolymer Thin Films. The all-dry iCVD synthesis approach was employed to synthesize amphiphilic copolymer thin films. iCVD is a solvent-free, free-radical polymerization technique known for its conformality, versatility, substrate independence, and nanoscale thickness control through *in situ* laser interferometry.[62] This technique allows researchers to deposit polymers with a wide range of functionalities, including hydrophilic and hydrophobic, hence creating amphiphilic coatings for antifouling application on any kind of substrate. iCVD enables the synthesis of amphiphilic copolymers with molecular heterogeneities for biofouling prevention.[49]

During iCVD, the monomer(s), inert gas, and initiator were metered into the reactor chamber under medium vacuum. After that, the physisorption of monomer(s) occurred at the cooled substrate. Once the filament array was turned on, TBPO decomposed to form *tert*-butoxy free radicals. Finally, once the radicals chemisorbed to the surface-adsorbed monomers, free-radical polymerization began, following the Eley−Rideal mechanism.[63] The sulfobetaine-based amphiphilic copolymers were fabricated by performing a post-deposition reaction with PS, in which the tertiary amine was converted to the quaternary ammonium group.

The homopolymers P4VP, PHFBA, PPFOA, P4VP-*co*-HFBA, and P4VP-*co*-PFOA thin films were also deposited by iCVD. The monomer gas fraction, f_{4VP}, was adjusted by changing P_m/P_{sat}, which is the ratio of monomer partial pressure over its saturated pressure at the specific stage temperature. Hence, P_m/P_{sat} is indicative of monomer surface concentration. All copolymers had a $P_{4VP}/P_{4VP,sat}$ range between 0.01 and 0.15 to avoid condensation and preserve coating conformality.

Characterization of the Amphiphilic Copolymer Thin Films. The successful synthesis of P4VP-*co*-HFBA and P4VP-*co*-PFOA copolymers was confirmed using FTIR spectroscopy and XPS. The FTIR spectra of homopolymers PHFBA and P4VP and copolymers with varying monomer gas fractions, f_{4VP}, are depicted in Figure 2a. The spectra for all samples were baseline-corrected and normalized by the film thickness. In Figure 2a, one of the characteristic peaks for PHFBA was the C═O stretching peak located at 1757 cm^{-1}. The absorption in the range of 1292−1190 cm^{-1} corresponded to the symmetric and asymmetric vibration of the CF_2 moiety, and the sharp peak at 1109 cm^{-1} was due to the CF_3 end group. The characteristic peaks for the P4VP homopolymer included the vibrations due to the pyridine ring from 1599 to 1415 cm^{-1} and the broad absorption at around 3000 cm^{-1} corresponding to alkyl C−H bonds, confirming the successful incorporation of 4VP into the polymer films.[64] The spectra of P4VP-*co*-HFBA copolymers with the 4VP surface composition (calculated using P_m/P_{sat} of 4VP and HFBA) ranging from 10.8 to 80.0% are also shown in Figure 2a. The presence of the characteristic absorptions of both the pyridine ring (at ∼1599 cm^{-1}) and the carbonyl group (at 1757 cm^{-1}) showed the incorporation of both 4VP and HFBA through the all-dry polymerization technique. It is also important to note that there was a slight shift in the peak position of the carbonyl group, that is, from 1757 cm^{-1} (for homopolymer PHFBA) to 1753 cm^{-1} (for the copolymers), confirming successful copolymerization rather than physical mixing of the homopolymers.[65]

Similarly, Figure 2b shows the FTIR spectra of P4VP-*co*-PFOA copolymers, with f_{4VP} ranging from 16.8 to 52.4%, and the corresponding homopolymers. PPFOA absorption peaks consisted of the carbonyl group (C═O) stretching at 1744 cm^{-1} and the asymmetric and symmetric stretching of CF_2 at 1238 cm^{-1} and 1203 cm^{-1}, respectively. Like PHFBA, there was a strong peak at 1146 cm^{-1} due to the CF_3 end group. P4VP-*co*-PFOA copolymers had characteristic peaks of both PFOA at 1740 cm^{-1} and 4VP at 1599 cm^{-1}, with C═O shifting from 1743 cm^{-1} (for homopolymer PPFOA) to 1740 cm^{-1} (for the copolymers), confirming copolymerization of P4VP-*co*-PFOA via iCVD.

The molar fraction of 4VP (F_{4VP}) in the copolymer (i.e., after the polymerization) differed from the feed composition (e.g., f_{4VP}) due to different reactivities of each monomer.[66] To calculate film composition from FTIR, Beer−Lambert's law was utilized with the assumption that the molar adsorption coefficients of the same characteristic peaks remained unchanged irrespective of the homopolymer or copolymer states.[67] Specifically, the copolymer compositions were

https://doi.org/10.1021/acssuschemeng.2c03933
ACS Sustainable Chem. Eng. XXXX, XXX, XXX−XXX

calculated using the area under the peak at 1599 cm^{-1} for the pyridine ring and the absorption at 1740−1757 cm^{-1} for the carbonyl group (see Supporting Information for details). From FTIR, the molar fraction for 4VP was calculated to be in the range of 35.4−85.1% for copolymers of P4VP-*co*-HFBA and 23.3−65.6% for copolymers of P4VP-*co*-PFOA (see Table 3).

Table 3. Comparison of Compositions of Copolymer Thin Films Obtained from FTIR and XPS

copolymer	f_{4VP} [%]	F_{4VP} (XPS) [%]	F_{4VP} (FTIR) [%]
P4VP-*co*-HFBA	10.8	39.8	35.4
	17.9	55.2	51.5
	29.8	63.2	57.8
	49.8	76.3	70.8
	66.4	81.1	77.8
	80.0	90.5	85.1
P4VP-*co*-PFOA	16.8	28.6	23.3
	30.3	51.9	45.4
	33.9	54.0	49.6
	52.4	67.1	65.6

To confirm those chemical compositions, XPS survey scans of P4VP-*co*-HFBA and P4VP-*co*-PFOA copolymer thin films with varying f_{4VP} were collected, as shown in Figure S1. All spectra captured peaks of C(1s) at 287 eV, O(1s) at 533 eV, N(1s) at 400 eV, and F(1s) at 690 eV. Compositions of the copolymer thin films were calculated using the ratio of the atomic percentage of fluorine to that of nitrogen to avoid the influence of adventitious carbon and oxygen (see Supporting Information for details). The surface compositions (because XPS is a surface-sensitive technique) of P4VP-*co*-HFBA copolymers were calculated to be in the range of 39.8−90.5%, with differences from those calculated using the FTIR spectra that were up to 5.5% (Table 3). Similarly, compositions of the P4VP-*co*-PFOA copolymers were calculated using the XPS results (Table 3), which were up to 6.5% different from the compositions obtained using the FTIR results. F_{4VP} (XPS) was consistently higher than F_{4VP} (FTIR) potentially due to the adventitious nitrogen. The composition results calculated using XPS were utilized to characterize the polymer thin films for biofilm quantification because the surface composition is the most relevant to antifouling applications.[68]

The high-resolution C(1s) spectra of the P4VP-*co*-HFBA copolymer thin films are shown in Figure 3a, with peak deconvolution shown in Figure 3b. The high-resolution C(1s) spectra of P4VP-*co*-HFBA copolymers could be fitted with six characteristic Gaussian peaks, located at 292.9, 290.4, 288.8, 285.6, 285.1, and 284.8 eV, corresponding to C−F_3, C−F_2, C−F, C═O, C−N, and C═C or C−C, respectively (Figure 3b). With the increasing 4VP content, the intensity of C−F_x peaks decreased, confirming the decrease in the amount of HFBA in the copolymers. The high-resolution C(1s) spectra of the P4VP-*co*-PFOA copolymer thin films and their peak deconvolution are shown in Figure 3c,d, respectively. The characteristic binding energies at 293.3, 291.1, 288.8, 285.4, and 284.8 eV corresponded to C−F_3, C−F, C═O, C−N, and C═C or C−C, respectively. The slight difference in binding energies of C−F_x peaks could be explained by the different chemical bonding environments in P4VP-*co*-PFOA versus

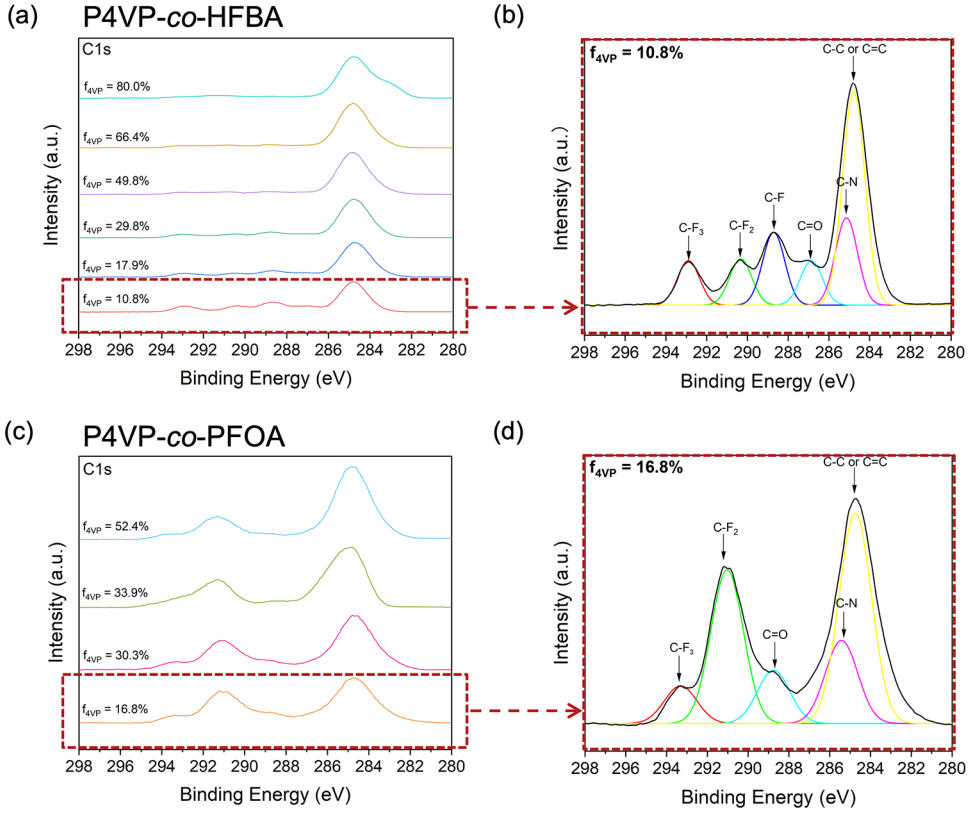

Figure 3. XPS high-resolution C(1s) spectra for (a) P4VP-*co*-HFBA copolymer thin films with varying f_{4VP}; (b) a P4VP-*co*-HFBA spectrum with f_{4VP} of 10.8% and peaks deconvoluted; (c) P4VP-*co*-PFOA copolymer thin films with varying f_{4VP}, and (d) a P4VP-*co*-PFOA spectrum with f_{4VP} of 16.8% and peaks deconvoluted. The samples were calibrated to the standard of 284.8 eV for C−C.

https://doi.org/10.1021/acssuschemeng.2c03933
ACS Sustainable Chem. Eng. XXXX, XXX, XXX−XXX

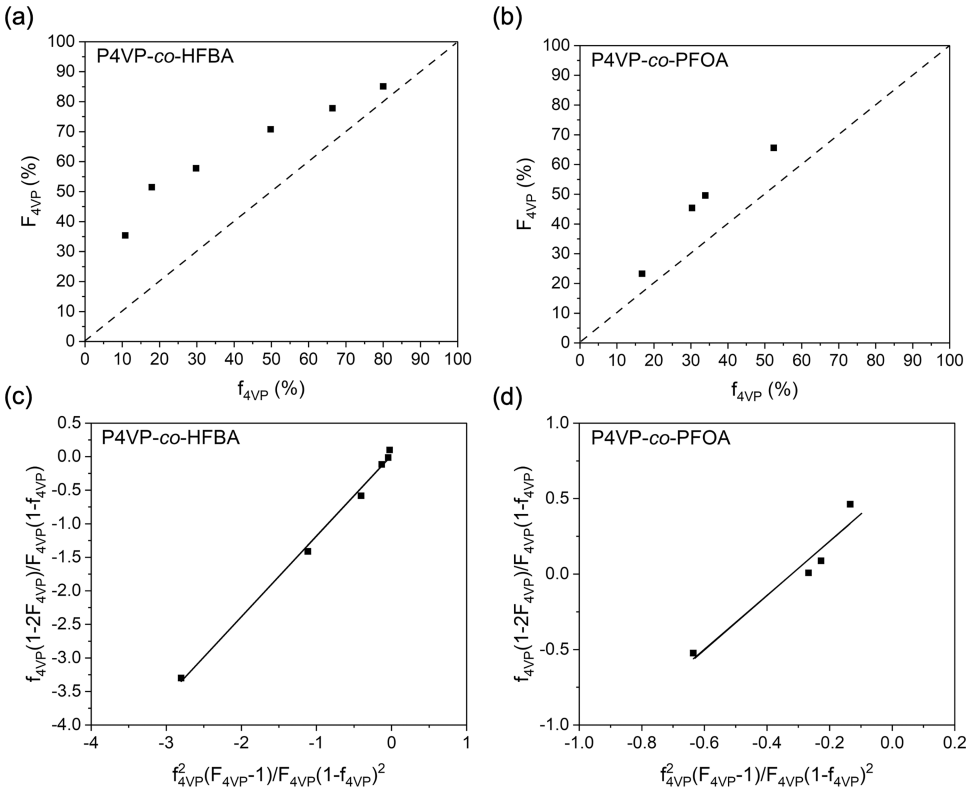

Figure 4. Copolymer analysis of P4VP-*co*-HFBA and P4VP-*co*-PFOA. The plot of the molar fraction of 4VP repeat units in the copolymers (F_{4VP}) as a function of the fraction of 4VP monomer at the substrate surface (f_{4VP}) for (a) P4VP-*co*-HFBA and (b) P4VP-*co*-PFOA copolymers. The Fineman−Ross copolymerization plot for (c) P4VP-*co*-HFBA and (d) P4VP-*co*-PFOA copolymer thin films.

P4VP-*co*-HFBA, that is, the absence of the C−F bond and additional C−C bond between the fluorinated chain and the ester group in the PFOA repeat units compared to HFBA.

Hence, polymer thin films of P4VP-*co*-HFBA and P4VP-*co*-PFOA were obtained via iCVD, the chemical compositions of which were adjusted across a wide range simply by varying the flow rate of each monomer.

Fineman−Ross Copolymerization Analysis and Formation of Nanodomains. To demonstrate that the copolymers P4VP-*co*-HFBA and P4VP-*co*-PFOA were statistical copolymers and hence have domain sizes on the nanoscale, reactivities of each co-monomer pairs were determined using the Fineman−Ross copolymerization analysis.[69]

The film compositions, indicated by the F_{4VP} values obtained from FTIR and thus representative of bulk film composition, were correlated with the monomer compositions at the substrate surface (f_{4VP}), where the polymerization occurred (Figure 4a,b). Interestingly, the compositions of 4VP in the copolymer thin films were slightly greater than its surface concentrations as monomers, hinting at a preference for the incorporation of 4VP into the copolymer compared to HFBA or PFOA. The Fineman−Ross equation was used to capture that preference quantitatively by correlating the film compositions with the surface monomer compositions. Take HFBA as an example, the Fineman−Ross equation is as follows

$$\frac{f_{4VP}(1-2F_{4VP})}{F_{4VP}(1-f_{4VP})} = r_{HFBA} + r_{4VP}\frac{f_{4VP}^2(F_{4VP}-1)}{F_{4VP}(1-f_{4VP})^2} \quad (1)$$

where r_{4VP} and r_{HFBA} were the reactivity ratios of 4VP and HFBA, respectively, which were obtained via linear regression of the compositional data (Figure 4a), as discussed below. If the resultant value of r_{4VP} is less than unity, it would suggest that a growing chain ending with a 4VP unit preferentially adds the HFBA monomer unit, while $r_{4VP} > 1$ would be indicative of a preference for self-addition. Hence, if r_{4VP} and r_{HFBA} are close to zero or $r_{4VP} \times r_{HFBA} \sim 0$, it would indicate that alternative copolymerization is likely, whereas $r_{4VP} > 1$ with $r_{HFBA} > 1$ implies block-like growth of chains.[69]

The plot for Fineman−Ross copolymerization equation for the copolymers P4VP-*co*-HFBA (Figure 4c) was used to determine the r_{4VP} and r_{HFBA}, which were found to be 1.20 and 0.02 ($R^2 = 0.99$), respectively, under the conditions detailed in Table 1. The r_{4VP} value of 1.20 indicated that statistically 4VP was more likely to react with itself, whereas the r_{HFBA} value of 0.02 indicated that HFBA was more likely to react with 4VP over another HFBA monomer. The preference for 4VP addition could be explained by its compact size and thus reduced steric hindrance compared to HFBA.[70] Furthermore, this preference for 4VP addition further implied that the fluorinated repeat unit was more likely to be surrounded by 4VP repeat units than to form a fluorinated block, hinting at a hydrophobic domain size that is close to the size of an HFBA monomer (estimated to be 1.2 nm for HFBA; see Figure S2). The fact that $r_{4VP} \times r_{HFBA} \sim 0.024 > 0$ suggests that iCVD polymerization followed a random behavior. Hence, the monomer residues were located randomly in the polymer molecule.

These reactivity ratios can be understood via the Q-e scheme, which is commonly used to predict reactivity ratios for liquid-phase free radical polymerization[71] based on the monomer resonance stabilization, Q_m, and a measure of monomer polar properties, e_m. For 4VP, Q_{4VP} was estimated to

https://doi.org/10.1021/acssuschemeng.2c03933
ACS Sustainable Chem. Eng. XXXX, XXX, XXX−XXX

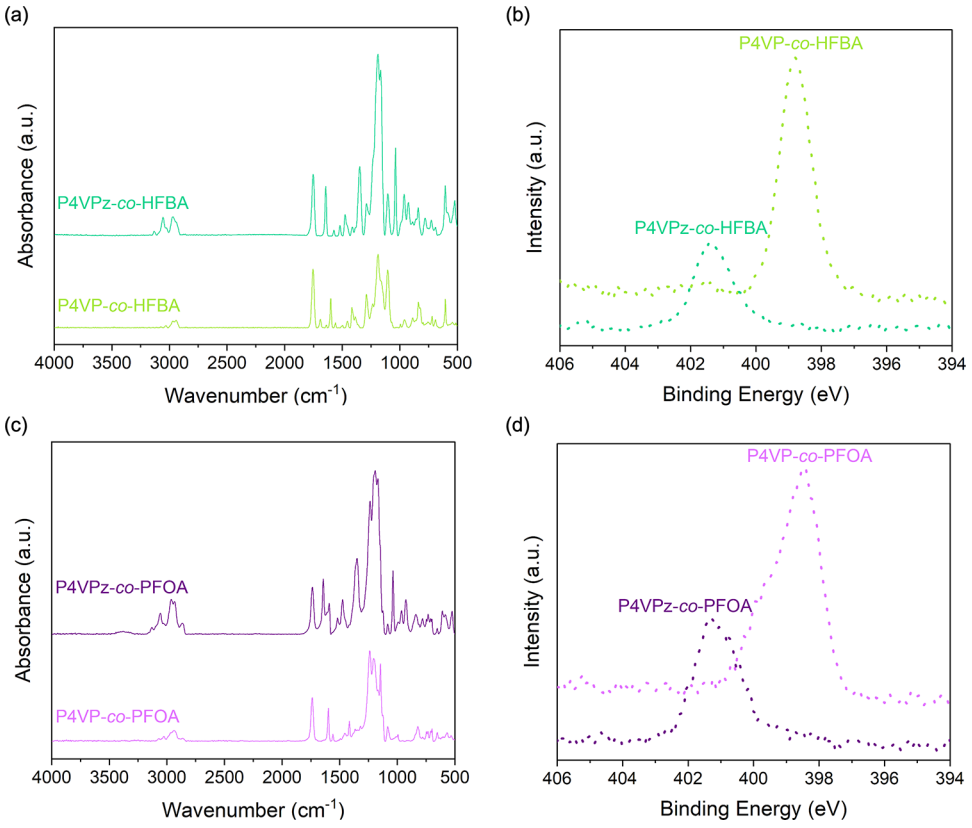

Figure 5. Chemical characterization of zwitterionic moieties in the amphiphilic copolymers. FTIR spectra of the copolymer before and after the PS reaction for (a) P4VP-*co*-HFBA and (c) P4VP-*co*-PFOA. XPS N(1s) high-resolution scans of (b) P4VP-*co*-HFBA and P4VPz-*co*-HFBA and (d) P4VP-*co*-PFOA and P4VPz-*co*-PFOA.

be 1.00 and e_{4VP} to be −0.28 using a database included in Odian's Principles of Polymerization;[69] while for HFBA, these parameters were estimated using the values for 2,2,3,4,4,4-hexafluorobutyl methacrylate (HFBMA),[72] due to unavailability of the data for HFBA (Q_{HFBMA} = 1.70, e_{HFBMA} = 1.24). Hence, the resultant predicted value for r_{4VP} was 0.38, while r_{HFBMA} was 0.26 for liquid-phase free radical polymerization. These values still pointed to the formation of random copolymers and the product of reactivity ratios: $r_{4VP} \times r_{HFBA}$ = 0.10, remained close to zero. That discrepancy between the experimentally derived r_{4VP} and the one predicted by the Q-e scheme could be attributed to the greater hydrophobicity of HFBA than HFBMA. The average water contact angle (WCA) for HFBMA is 114°,[73] and for HFBA, it is 121°.[74] In addition, kinetic rate constants of iCVD polymerization and those for solution-phase polymerization could differ,[75] which may also contribute to that discrepancy.

A similar analysis was performed on copolymers of 4VP and PFOA. Figure 4d shows the Fineman−Ross copolymerization plot for P4VP-*co*-PFOA copolymers, from which the reactivity ratios of 4VP and PFOA, that is, r_{4VP} and r_{PFOA}, were determined to be 1.79 and 0.57, respectively (R^2 = 0.94), indicating the formation of random copolymers with a preference for 4VP addition, similar to P4VP-*co*-HFBA copolymers. The higher values for r_{4VP} and r_{PFOA} in P4VP-*co*-PFOA than those in P4VP-*co*-HFBA can be attributed to the higher hydrophobicity of PFOA. Nevertheless, the implication remains that a fluorinated repeat unit was likely surrounded by 4VP repeat units, giving rise to random heterogeneous copolymers and hydrophobic nanodomains (estimated to be 1.9 nm; see Figure S2).

The amphiphilic random copolymers, P4VP-*co*-HFBA and P4VP-*co*-PFOA, are novel chemistries enabled by the iCVD technique. The all-dry synthesis conditions circumvented microphase separation to achieve heterogeneities on the molecular level without the need for a common solvent.[76]

Formation of Zwitterionic Moieties. 4VP has been used to produce zwitterionic moieties via a vapor-phase reaction with PS.[77−79] The reaction proceeded through a ring-opening mechanism, in which the pyridine nitrogen was quaternized and a pyridinium-based sulfobetaine group was formed. It is beneficial to have amphiphilic copolymers with zwitterionic groups to increase the contrast in surface energy between the hydrophilic and hydrophobic repeat units in amphiphilic chemistry, an effective approach to improve the antifouling performance at the air−liquid−solid interface.

The vapor-phase ring-opening reaction was first performed on a P4VP polymer, which was lightly crosslinked with DVB (with a DVB content of 7.5% to render the zwitterionic polymer stable and insoluble in water), using an established procedure.[77−79] To confirm that the PS reaction was successful, FTIR and XPS high-resolution N(1s) spectra were collected before and after the reaction. Figure S3 depicts FTIR spectra for P4VP and its zwitterionic derivative (P4VPz). New peaks were observed at 1194 and 1036 cm^{-1}, which corresponded to the SO_3^- group in the pyridinium-based zwitterionic moieties. In addition, a new peak formed at 1641 cm^{-1} corresponding to the quaternized pyridinium nitrogen.

https://doi.org/10.1021/acssuschemeng.2c03933
ACS Sustainable Chem. Eng. XXXX, XXX, XXX−XXX

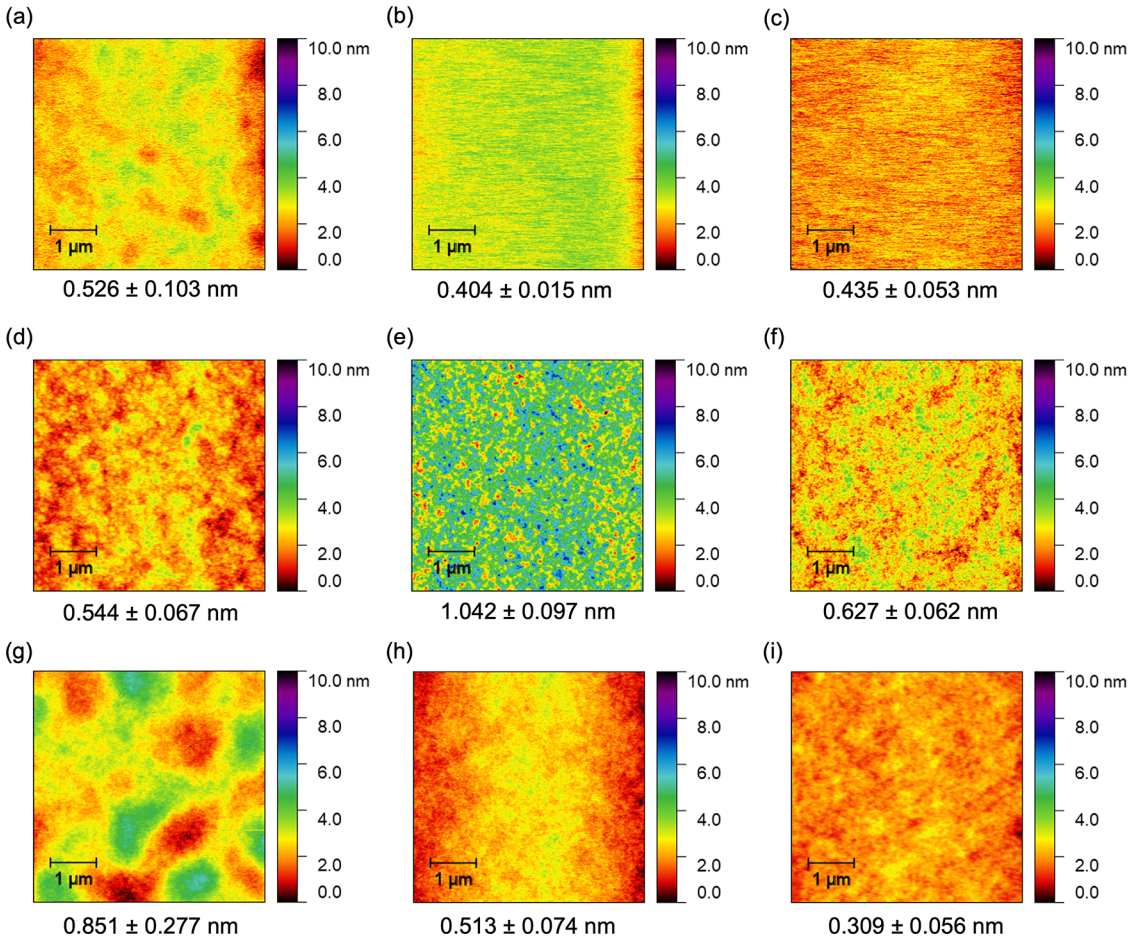

Figure 6. Atomic force microscopy height images of a 5 × 5 μm view of iCVD polymer coatings of (a) P4VP, (b) PHFBA, (c) PPFOA, and (d–f) P4VP-*co*-HFBA thin films with F_{4VP} of 63.2, 76.3, and 90.5%, respectively; (g) P4VPz, (h) P4VPz-*co*-HFBA, and (i) P4VPz-*co*-PFOA. The RMS surface roughness is shown under each image. Data = Mean ± SD, n = 2.

Prior reports have demonstrated that for random amphiphilic copolymers, the composition of 50% hydrophilic and 50% hydrophobic repeat units leads to the greatest antifouling performance.[38,39] Therefore, we chose the amphiphilic copolymers with compositions of around 50% of each monomer to perform the vapor-phase PS reaction to convert the 4VP repeat units into zwitterionic moieties. Figure 5a depicts the FTIR spectra of amphiphilic P4VP-*co*-HFBA (55.2% 4VP) and its zwitterionic derivative. Again, the new peak at 1037 cm^{-1} corresponded to the sulfonate group, and the peak shift of the pyridine ring from 1601 to 1645 cm^{-1} indicated that all nitrogens were fully quaternized. Figure 5b depicts XPS spectra of high-resolution N(1s) before and after PS treatment. N(1s) in P4VP-*co*-HFBA had a binding energy of 398.8 eV, which was representative of the pyridine ring. It shifted to 401.4 eV for P4VPz-*co*-HFBA due to the quaternization of the pyridine nitrogen. Figure 5c depicts the FTIR spectra of P4VP-*co*-PFOA (54.0% 4VP) and P4VPz-*co*-PFOA. Similar to P4VP-*co*-HFBA, near-complete reaction conversion was confirmed through the presence of a sulfonate peak at 1037 cm^{-1} and a pyridinium peak at 1643 cm^{-1}. Lastly, Figure 5d shows high-resolution N(1s) spectra for P4VP-*co*-PFOA and P4VPz-*co*-PFOA, where the peak shift from 398.4 to 401.3 eV confirmed the successful creation of zwitterionic moieties. Therefore, FTIR and XPS analyses confirmed successful syntheses of amphiphilic copolymers made of repeat units bearing zwitterionic moieties and fluorinated side chains.

Lastly, to confirm the insolubility of the amphiphilic coatings, the reacted samples were soaked in Milli-Q water over a period of 8 h at 37 °C, and the polymer thin film thickness before and after the incubation was measured using ellipsometry. The results are summarized in Table S1. The thickness change was below 10% for all samples despite small reductions (e.g., 6.4% for P4VPz-*co*-HFBA and 2.1% for P4VPz-*co*-PFOA), which was likely a result of chain reorganizations (e.g., reduction of free volume) during the soaking and drying procedures. Thus, the aforementioned characterizations confirmed the successful synthesis of stable and insoluble amphiphilic thin films.

Surface Topography of the iCVD Thin Films. Surface topography is known to play a crucial yet controversial role in bacterial adhesion and biofilm formation.[80] While most of the existing antibiofouling reports focus on surface roughness on the micrometer scale, we refer the readers to the rich body of literature[81−87] for a detailed discussion on that topic and focus our discussion here on the length scale that is relevant to iCVD coatings, that is, on the order of 0.1 nm to 100 nm.[26,38,75,88] At this length scale, lower surface roughness has been considered desirable for reducing biofilm formation. A recent report has made the observation that a hydrophobic surface with a root mean square (RMS) roughness of 1 nm led to an amount of *S. aureus* adhesion that was merely 2% that of a surface with an RMS roughness of 205 nm.[89] Hydrophobic surfaces with nanoroughness ranging from 2.28 to 28.35 nm have been

https://doi.org/10.1021/acssuschemeng.2c03933
ACS Sustainable Chem. Eng. XXXX, XXX, XXX−XXX

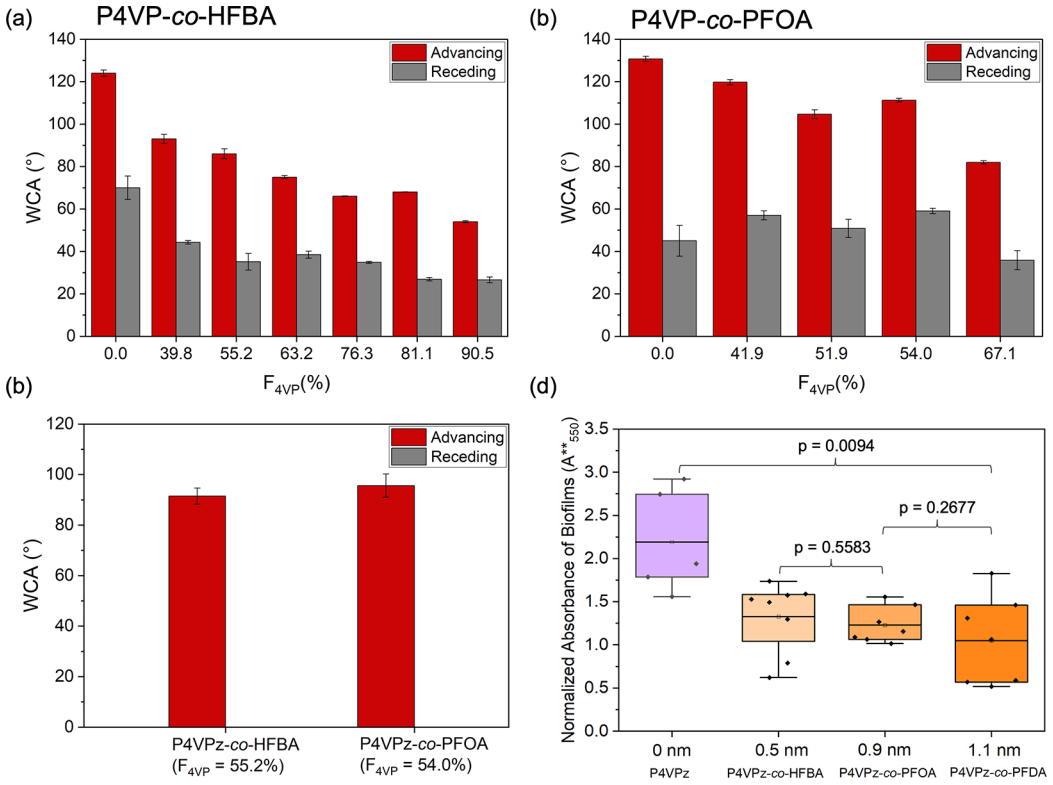

Figure 7. Advancing and receding WCA measurements for (a) PHFBA and P4VP-*co*-HFBA copolymers; (b) PPFOA and P4VP-*co*-PFOA copolymers; and (c) P4VPz-*co*-HFBA and P4VPz-*co*-PFOA. The receding WCA was zero for these two copolymers. (d) Biofilm formation on the amphiphilic copolymer thin films. Normalized absorbance of biofilms for P4VPz and amphiphilic copolymers with different lengths of the perfluorinated side chain (P4VPz-*co*-HFBA, P4VPz-*co*-PFOA, and P4VPz-*co*-PFDA). P4VPz-*co*-PFDA data were reproduced with permission from ref 38. Copyright 2021 Wiley.

shown to deter the attachment of *Cellulophaga lytica*, *Ulva*, and *Navicula incerta*.[90] Similar observations have been made and attributed to the Cassie-Baxter wetting state,[91] which reduced the contact area between the surface and bacteria foulants. Nevertheless, that preference for lower surface roughness in antibiofilm applications is by no means a consensus, as numerous reports have observed increased bacterial adhesion at lower roughness for hydrophilic titanium surfaces,[92−94] which has been attributed to enhanced production of the extracellular polymeric substance on smooth hydrophilic surfaces.[95] In one study, an RMS roughness of 0.16 μm was discovered to be optimum (in the range of 0.03−0.89 μm) for hydrophilic surfaces to achieve biofilm reduction when tested using *D. desulfuricans, P. putida, P. aeruginosa,* and *Rhodococcus*.[96] With that controversy in mind, it is important to evaluate surface roughness of the iCVD amphiphilic copolymers to add more data points to the observations of possible impacts of surface morphology on bacterial biofilm formation. To characterize the surface topography of the polymer thin films, AFM was used in AC air mode, and Figure 6 depicts height images of P4VP, PHFBA, and PPFOA homopolymers, P4VP-*co*-HFBA copolymers with varying 4VP compositions, and the polymers bearing zwitterionic side groups (i.e., P4VPz, P4VPz-*co*-HFBA, and P4VPz-*co*-PFOA).

Homopolymers depicted in Figure 6a−c were extremely smooth with RMS roughness below 1 nm, confirming the smoothness of the iCVD polymers.[75] While perfluorinated polymers with long chains synthesized by iCVD, for example, PPFDA, tend to form crystalline structures with RMS roughness >30 nm,[97−99] thus creating rough surfaces, as compared to more common iCVD polymer thin films with surface roughness <1 nm.[75,100,101] The fluorinated polymers synthesized here, with their fluorinated chain lengths of 3 (HFBA) and 6 (PFOA) did not show any crystallinity,[65] as demonstrated by X-ray diffraction (XRD) (Figure S4).[102]

For the P4VP-*co*-HFBA copolymers, the RMS roughness was 0.544 ± 0.067 nm for F_{4VP} of 63.2%, 1.042 ± 0.097 nm for F_{4VP} of 76.3%, and 0.627 ± 0.062 nm for F_{4VP} of 90.5% 4VP (Figure 6d−f). The greater roughness for the copolymer samples than that of homopolymer samples could be attributed to the instability caused by the copolymerization of monomers with contrasting surface energies.[38,39] The surface roughness demonstrated by the iCVD copolymers was still much smaller than the counterparts synthesized using solution-based methods.[103,104]

Lastly, the surface roughness of the reacted copolymers remained low (Figure 6g−i), with RMS roughness values below 1 nm, which represents some of the smoothest amphiphilic copolymers produced via iCVD. In the previous studies, the lowest RMS roughness was ∼21.6 nm for P4VPz-*co*-PFDA[38] and ∼2−5 nm for PHEMA-*co*-PFDA.[39] This exceptional smoothness of *the* P4VPz-*co*-HFBA and P4VPz-*co*-PFOA could be explained by the absence of crystallinity of the hydrophobic monomers and improved mixing of the hydrophobic monomer and the precursor monomer (i.e., 4VP, as a precursor for the zwitterionic moiety) during iCVD. The absence of crystallinity was confirmed by performing XRD on the P4VPz-*co*-HFBA and P4VPz-*co*-PFOA copolymers (Figure S5), which demonstrated no discernable crystal structures. This minimal surface roughness is beneficial for antifouling

https://doi.org/10.1021/acssuschemeng.2c03933
ACS Sustainable Chem. Eng. XXXX, XXX, XXX−XXX

effectiveness because it prevents the roughness-induced adhesion strength of marine organisms.[105]

Dynamic WCA Evaluation. The dynamic wetting behavior, which has been shown to be critical for achieving antibiofouling effectiveness at the air−liquid−solid interface,[38] was assessed via dynamic WCA measurements. Figure 7a depicts advancing and receding WCA for P4VP-*co*-HFBA thin films with varying F_{4VP}. The homopolymer of HFBA had an advancing WCA of 123.6 ± 1.5° with a receding WCA of 70.0 ± 5.5°, confirming the hydrophobicity of HFBA with significant hysteresis of 53.6 °. Such a large hysteresis was attributed to the reorientation of the fluorinated side chains when transitioning from a dry state (with the fluorinated side chains pointing to the topmost surface) to a wetted state (with the fluorinated side chains buried in the bulk film to minimize interfacial energy).[65] With the increase of F_{4VP} from 39.8 to 90.5%, the advancing WCA decreased from 123.6 ± 1.5° to 54.3 ± 0.4° due to the presence of more hydrophilic domains; the receding WCA similarly dropped from 44.3 ± 0.8° to 26.6 ± 1.4°. The receding WCA was below 40° for samples with F_{4VP} > 39.8%. The large WCA hysteresis confirmed the amphiphilic nature of P4VP-*co*-HFBA, which could reorient the fluorinated side chains based on the wetting condition, that is, demonstrating hydrophobicity at the liquid−air interface and hydrophilicity at the liquid−solid interface.

Figure 7b shows dynamic WCA measurement for P4VP-*co*-PFOA copolymers with varying F_{4VP}. The homopolymer of PFOA had an advancing WCA of 130.7 ± 1.2°, which was slightly larger than that of PHFBA due to PFOA's longer fluorinated chain. The receding WCA was 45.0 ± 7.3° and the hysteresis was 85.7°, which could be explained by the facile chain reorientation of PFOA, likely enabled by the flexible $-C_2H_4-$ linker connecting the fluorinated moieties to the acrylate backbone. With the increase of F_{4VP} from 41.9 to 67.1%, the advancing WCA dropped from 130.7 ± 1.2° to 82.0 ± 0.8° and the receding WCA decreased from 57.0 ± 2.1° to 35.9 ± 4.5°. The WCA hysteresis reduced to 46.1° upon the incorporation of 4VP at F_{4VP} of 33.9%, which was likely due to the reduced amount of the fluorinated side chains that can reorient quickly. The WCA hysteresis subsequently increased to 62.8° for F_{4VP} of 58.1%, which was a result of the molecular-level heterogeneity that was maximized around this composition.

Lastly, Figure 7c depicts the dynamic WCA for the reacted amphiphilic copolymers, that is, P4VPz-*co*-HFBA (F_{4VP} of 55.2%) and P4VPz-*co*-PFOA (F_{4VP} of 54.0%). The advancing WCA was 91.5 ± 3.2° for P4VPz-*co*-HFBA and 95.6 ± 4.6° for P4VPz-*co*-PFOA, comparable to those of the unreacted P4VP-*co*-HFBA and P4VP-*co*-PFOA (85.7 ± 2.3° and 104.7 ± 2.0°, respectively). The change in the advancing WCA was insignificant (<10°), thus indicating that the copolymers retained similar hydrophobicity at the solid−air interface after the treatment, further corroborating the facile surface chain reorientation. The receding WCA values for both reacted samples were close to zero, confirming the superhydrophilicity of zwitterionic moieties at the solid−liquid interface.

Antifouling Performance at the Solid−Liquid−Air Interface. The antifouling performance of the amphiphilic thin films was tested using *P. aeruginosa,* strain PAO1, because it is one of the most common strains used to form a biofilm,[106] and it is known for the tendency to grow a biofilm at the solid−liquid−air interface. Figure 7d depicts the results of biofilm formation on the amphiphilic copolymers with different hydrophobic chain lengths ranging from 0.5 to 1.1 nm: P4VPz-*co*-HFBA, P4VPz-*co*-PFOA, and P4VPz-*co*-PFDA (reproduced from the previous study).[38] The zwitterionic coating P4VPz was used as a point of comparison for its well-established fouling resistance. The absorbance of the biofilm at 550 nm (OD_{550}, obtained by CV straining and subsequent biofilm solubilization) was normalized by the OD_{600} of the culture to account for potential variations in the inoculation density and culture conditions (i.e., A_{550}/A_{600}). That absorbance was further normalized by the OD_{550}/OD_{600} of clean unmodified glass slides (i.e., A^*_{550}/A^*_{600}) to prevent any potential variations in the substrate conditions to obtain the final value of A^{**}_{550}. It is important to note that we chose glass as the benchmark of comparison based on its exceptional antifouling performance.[79,107] However, glass is also unlikely to be used as a versatile antifouling coating and its inclusion here is merely for benchmarking.

All amphiphilic copolymers outperformed the zwitterionic coating, with an average improvement of 45% compared to P4VPz. Despite the small variations in terms of their antibiofilm performance among the amphiphilic copolymers (i.e., P4VPz-*co*-HFBA, P4VPz-*co*-PFOA, and P4VPz-*co*-PFDA), there was no statistical significance to those variations, as indicated by the large *p*-value labeled in Figure 7d. On average, P4VPz-*co*-PFDA (with a perfluorinated chain length of ∼1.1 nm) led to biofilm growth that was 47.9 ± 27.7% that of P4VPz, whereas P4VPz-*co*-HFBA (with a perfluorinated chain length of ∼0.5 nm) and P4VPz-*co*-PFOA (with a perfluorinated chain length of ∼0.9 nm) resulted in biofilm growth that was 60.7 ± 22.9% and 56.2 ± 16.5% that of P4VPz, respectively. While the excellent antifouling performance of p4VPz at the liquid−solid interface has been well established in the literature,[108−111] P4VPz incurred an amount of the PAO1 biofilm that was near twice the amount on glass at the solid−liquid−air interface. In contrast, the statistical amphiphilic copolymers, P4VPz-*co*-HFBA, P4VPz-*co*-PFOA, and P4VPz-*co*-PFDA, demonstrated comparable antibiofilm performance as glass, indicating good fouling resistance.[79,107] Hence, it could be concluded that the length of the fluorinated chain in statistical amphiphilic copolymers did not modify their antibiofilm effectiveness significantly when varied in the range of 0.5−1.1 nm. Thus, it was possible to achieve similar antibiofilm performance with a shorter fluorinated side chain like that of HFBA, while reducing the environmental impact of fluorine-based amphiphilic antifouling coatings. Furthermore, the RMS roughness of P4VPz-*co*-PFDA has been reported to be ∼21.6 nm,[38] while its antibiofilm performance was found to be comparable to that of P4VPz-*co*-HFBA and of P4VPz-*co*-PFOA (Figure 7d), thus corroborating the insignificant impact of nanometer-scale surface roughness of the statistical amphiphilic coatings on PAO1 biofilm formation.

To demonstrate that the good antibiofilm performance was not a result of the leaching of toxic constituents from the iCVD thin films, we incubated PHFBA and PPFOA in LB medium for 8 h at 37 °C. FTIR spectra were taken before and after the 8-h incubation (Figure S6). Reduction of peak intensities in FTIR was undetectable, indicating very little release of constituents from the iCVD amphiphilic thin films into LB medium over the course of 8 h. The slight increase in the intensities of a few peaks (e.g., the peak at 1757/1743 cm^{-1}) can be explained by (i) reorientation of the fluorinated side chains, which is known to occur upon wetting and drying of

https://doi.org/10.1021/acssuschemeng.2c03933
ACS Sustainable Chem. Eng. XXXX, XXX, XXX−XXX

the thin film[65] and (ii) adsorption of constituents of the LB medium into the thin film.

CONCLUSIONS

In this study, amphiphilic copolymers were synthesized using a hydrophilic pyridinium-based zwitterionic monomer and a hydrophobic monomer bearing a fluorinated size chain with less than 7 fluorocarbons, that is, HFBA or PFOA. The short-chain fluorinated monomers were selected because the chemicals containing long-chain perfluoroalkyl groups (C_nF_{2n+1}, $n \geq 7$) are known to be global contaminants, causing bioaccumulation, toxicity, and persistent distribution in the environment.[112] Statistical copolymers of 4VP, the precursor of the pyridinium-based zwitterionic moieties, and HFBA or PFOA were obtained by a solvent-free vapor deposition technique, iCVD. The random copolymerization was deduced from the Fineman−Ross analysis, hinting at hydrophobic domains at the nanoscale and the absence of microphase separation. The copolymers of 4VP and HFBA or PFOA were subsequently converted to amphiphilic copolymers by a vapor treatment with PS, turning the pyridine rings in 4VP into pyridinium-based zwitterionic moieties. We hypothesized that the amphiphilic copolymers could resist biofilm formation at the air−liquid−solid interface because of the facile chain reorientation at the triple interface, presenting a hydrophobic surface at the air−solid interface and a hydrophilic one at the liquid−solid interface. That facile chain reorientation was proven by dynamic WCA measurements, where the advancing WCA remained unchanged upon converting 4VP into zwitterions (which is more hydrophilic than 4VP), indicating that the dry-state surface energy was dictated by the fluorinated side chains. The good antibiofilm antifouling performance of the two amphiphilic copolymers at the triple interface was demonstrated using *P. aeruginosa* strain PAO1. Even the amphiphilic copolymer made with HFBA (with three fluorinated carbon atoms) outperformed a purely zwitterionic coating by 39.3%, as evaluated by the quantity of biofilms formed on each surface; whereas the one made with PFOA had merely 56.2 ± 16.5% the amount of biofilm on the purely zwitterionic coating. As such, less bioaccumulative and less toxic amphiphilic coatings have been successfully synthesized and demonstrated to be antibiofilm, greatly accelerating the deployment of similar chemistries in a broad cross-section of industries ranging from food manufacturing to healthcare. Our future research will focus on the development of fluorine-free amphiphilic coatings to further reduce the potential side effects of fluorocarbon chemistry. Research into biofouling prevention at the triple interface is still in its infancy and many critical questions remain to be answered, including the relative impact of the triple interface with respect to hydrodynamic drag, larval recruitment, and cleanability/sloughing potential. We believe that these questions are instrumental for the continued development of biofouling prevention measures at the triple interface and predict that the impact of biofouling prevention at the triple interface is significant, especially given its prevalence in propellers and heat exchangers.[113] Future evaluation of antifouling performance under natural or environmental conditions like seawater would provide a realistic assessment of the performance and durability of the amphiphilic copolymer coatings. Those tests would likely require careful examination and selection of the model strains like *V. cyclitrophicus*, which has been used in antibiofouling studies due to its prevalence in coastal seawater and consistent growth under laboratory conditions.[57]

ASSOCIATED CONTENT

Supporting Information

The Supporting Information is available free of charge at https://pubs.acs.org/doi/10.1021/acssuschemeng.2c03933.

Calculation of monomer fraction at the substrate surface, calculation of copolymer composition from FTIR and XPS, 3D structures of monomers, XPS survey scans, FTIR spectra of P4VP and P4VPz, XRD for homopolymers and copolymers, and evaluation of the stability of the coatings (PDF)

AUTHOR INFORMATION

Corresponding Author

Rong Yang − *Robert Frederick Smith School of Chemical and Biomolecular Engineering, Cornell University, Ithaca, New York 14853, United States;* orcid.org/0000-0001-6427-026X; Email: ryang@cornell.edu

Authors

Alexandra Khlyustova − *Robert Frederick Smith School of Chemical and Biomolecular Engineering, Cornell University, Ithaca, New York 14853, United States;* orcid.org/0000-0002-4313-5066

Mia Kirsch − *Robert Frederick Smith School of Chemical and Biomolecular Engineering, Cornell University, Ithaca, New York 14853, United States*

Complete contact information is available at: https://pubs.acs.org/10.1021/acssuschemeng.2c03933

Notes

The authors declare no competing financial interest.

ACKNOWLEDGMENTS

This project is sponsored by the Department of the Navy, Office of Naval Research (ONR) award N00014-20-1-2418. This work made use of the Cornell Center for Materials Research (CCMR) Shared Facilities, which are supported through the NSF MRSEC program (DMR-1719875).

REFERENCES

(1) Hofmann, A.; van Strien, W. J.Maintaining Well & Facility Health − The Application of DNA Analysis to Corrosion and Bio-Fouling Prevention. In *Offshore Mediterranean Conference and Exhibition 2019*; 2019; pp 1−13.

(2) Goudie, M. J.; Pant, J.; Handa, H. Liquid-Infused Nitric Oxide-Releasing (LINORel) Silicone for Decreased Fouling, Thrombosis, and Infection of Medical Devices. *Sci. Rep.* **2017**, *7*, 13623.

(3) Damodaran, V. B.; Murthy, S. N. Bio-Inspired Strategies for Designing Antifouling Biomaterials. *Biomater. Res.* **2016**, *20*, 18.

(4) Wu, Y.; Xia, Y.; Jing, X.; Cai, P.; Igalavithana, A. D.; Tang, C.; Tsang, D. C. W.; Ok, Y. S. Recent Advances in Mitigating Membrane Biofouling Using Carbon-Based Materials. *J. Hazard. Mater.* **2020**, *382*, No. 120976.

(5) Demirel, Y. K.; Song, S.; Turan, O.; Incecik, A. Practical Added Resistance Diagrams to Predict Fouling Impact on Ship Performance. *Ocean Eng.* **2019**, *186*, No. 106112.

(6) Blenkinsopp, S. A.; Khoury, A. E.; Costerton, J. W. Electrical Enhancement of Biocide Efficacy against Pseudomonas Aeruginosa Biofilms. *Appl. Environ. Microbiol.* **1992**, *58*, 3770−3773.

(7) Yebra, D. M.; Kiil, S.; Dam-Johansen, K. Antifouling Technology - Past, Present and Future Steps towards Efficient and Environ-

mentally Friendly Antifouling Coatings. *Prog. Org. Coat.* **2004**, *50*, 75−104.
(8) Donadt, T. B.; Yang, R. Vapor-Deposited Biointerfaces and Bacteria : An Evolving Conversation. *ACS Biomater. Sci. Eng.* **2020**, *6*, 182−197.
(9) Russell, A. D. Similarities and Differences in the Responses of Microorganisms to Biocides. *J. Antimicrob. Chemother.* **2003**, *52*, 750−763.
(10) Ma, X.; Lang, J.; Chen, P.; Yang, R. Silver Nanoparticles as an Effective Antimicrobial against Otitis Media Pathogens. *AIChE J.* **2021**, *67*, No. e17468.
(11) Porter, R.; Miale, J. B. Extended Control of Marine Fouling Formulation of a Microencapsulated Liquid Organometallic Biocide and Vinyl Rosin Paint. *Appl. Biochem. Biotechnol.* **1984**, *9*, 439−445.
(12) Nehring, S. Long-Term Changes in Prosobranchia (Gastropoda) Abundances on the German North Sea Coast: The Role of the Anti-Fouling Biocide Tributyltin. *J. Sea Res.* **2000**, *43*, 151−165.
(13) Ytreberg, E.; Karlsson, J.; Eklund, B. Comparison of Toxicity and Release Rates of Cu and Zn from Anti-Fouling Paints Leached in Natural and Artificial Brackish Seawater. *Sci. Total Environ.* **2010**, *408*, 2459−2466.
(14) Srinivasan, R.; Stewart, P. S.; Griebe, T.; Chen, C.-I.; Xu, X. Biofilm Parameters Influencing Biocide Efficacy. *Biotechnol. Bioeng.* **1995**, *46*, 553−560.
(15) Flach, C. F.; Pal, C.; Svensson, C. J.; Kristiansson, E.; Östman, M.; Bengtsson-Palme, J.; Tysklind, M.; Larsson, D. G. J. Does Antifouling Paint Select for Antibiotic Resistance? *Sci. Total Environ.* **2017**, *590−591*, 461−468.
(16) Gomes, I. B.; Simões, M.; Simões, L. C. Copper Surfaces in Biofilm Control. *Nanomaterials* **2020**, *10*, 2491.
(17) Reddy, S.; Kaur, K.; Barathe, P.; Shriram, V.; Govarthanan, M.; Kumar, V. Antimicrobial Resistance in Urban River Ecosystems. *Microbiol. Res.* **2022**, *263*, No. 127135.
(18) Silva, I.; Tacão, M.; Henriques, I. Selection of Antibiotic Resistance by Metals in a Riverine Bacterial Community. *Chemosphere* **2021**, *263*, No. 127936.
(19) Wales, A. D.; Davies, R. H. Co-Selection of Resistance to Antibiotics, Biocides and Heavy Metals, and Its Relevance to Foodborne Pathogens. *Antibiotics* **2015**, *4*, 567−604.
(20) Singha, P.; Locklin, J.; Handa, H. A Review of the Recent Advances in Antimicrobial Coatings for Urinary Catheters. *Acta Biomater.* **2017**, *50*, 20−40.
(21) Chen, S.; Li, L.; Zhao, C.; Zheng, J. Surface Hydration: Principles and Applications toward Low-Fouling/Nonfouling Biomaterials. *Polymer* **2010**, *51*, 5283−5293.
(22) Singha, P.; Pant, J.; Goudie, M. J.; Workman, C. D.; Handa, H. Enhanced Antibacterial Efficacy of Nitric Oxide Releasing Thermoplastic Polyurethanes with Antifouling Hydrophilic Topcoats. *Biomater. Sci.* **2017**, *5*, 1246−1255.
(23) He, M.; Gao, K.; Zhou, L.; Jiao, Z.; Wu, M.; Cao, J.; You, X.; Cai, Z.; Su, Y.; Jiang, Z. Zwitterionic Materials for Antifouling Membrane Surface Construction. *Acta Biomater.* **2016**, *40*, 142−152.
(24) Khlyustova, A.; Cheng, Y.; Yang, R. Vapor-Deposited Functional Polymer Thin Films in Biological Applications. *J. Mater. Chem. B* **2020**, *8*, 6588−6609.
(25) Chen, P.; Lang, J.; Zhou, Y.; Khlyustova, A.; Zhang, Z.; Ma, X.; Liu, S.; Cheng, Y.; Yang, R. An Imidazolium-Based Zwitterionic Polymer for Antiviral and Antibacterial Dual Functional Coatings. *Sci. Adv.* **2022**, *8*, No. eabl8812.
(26) Khlyustova, A.; Kirsch, M.; Ma, X.; Cheng, Y.; Yang, R. Surfaces with Antifouling-Antimicrobial Dual Function via Immobilization of Lysozyme on Zwitterionic Polymer Thin Films. *J. Mater. Chem. B* **2022**, *10*, 2728−2739.
(27) Vilain, S.; Pretorius, J. M.; Theron, J.; Brözel, V. S. DNA as an Adhesin: Bacillus Cereus Requires Extracellular DNA to Form Biofilms. *Appl. Environ. Microbiol.* **2009**, *75*, 2861−2868.
(28) Medrano-Félix, J. A.; Chaidez, C.; Mena, K. D.; del S. Soto-Galindo, M.; Castro-Del Campo, N. Characterization of Biofilm Formation by Salmonella Enterica at the Air−Liquid Interface in Aquatic Environments. *Environ. Monit. Assess.* **2018**, *190*, 221.
(29) Spiers, A. J.; Bohannon, J.; Gehrig, S. M.; Rainey, P. B. Biofilm Formation at the Air−Liquid Interface by the Pseudomonas Fluorescens SBW25 Wrinkly Spreader Requires an Acetylated Form of Cellulose. *Mol. Microbiol.* **2003**, *50*, 15−27.
(30) Martí, S.; Rodríguez-Bão, J.; Catel-Ferreira, M.; Jouenne, T.; Vila, J.; Seifert, H.; Dé, E. Biofilm Formation at the Solid−Liquid and Air−Liquid Interfaces by Acinetobacter Species. *BMC Res. Notes* **2011**, *4*, 5.
(31) Ma, W.; Peng, D.; Walker, S. L.; Cao, B.; Gao, C. H.; Huang, Q.; Cai, P. Bacillus Subtilis Biofilm Development in the Presence of Soil Clay Minerals and Iron Oxides. *NPJ Biofilms Microbiomes* **2017**, *3*, 4.
(32) Sanchez-Vizuete, P.; Dergham, Y.; Bridier, A.; Deschamps, J.; Dervyn, E.; Hamze, K.; Aymerich, S.; le Coq, D.; Briandet, R. The Coordinated Population Redistribution between Bacillus Subtilis Submerged Biofilm and Liquid-Air Pellicle. *Biofilm* **2022**, *4*, No. 100065.
(33) Alavi, M. R.; Shukla, H. D.; Whitaker, B.; Arnold, J.; Shahamat, M. Attachment and Biofilm Formation of Mycobacterium Marinum on a Hydrophobic Surface at the Air Interface. *World J. Microbiol. Biotechnol.* **2007**, *23*, 93−101.
(34) Vestby, L. K.; Møretrø, T.; Langsrud, S.; Heir, E.; Nesse, L. L. Biofilm Forming Abilities of Salmonella Are Correlated with Persistence in Fish Meal- and Feed Factories. *BMC Vet. Res.* **2009**, *5*, 20.
(35) Wijman, J. G. E.; de Leeuw, P. P. L. A.; Moezelaar, R.; Zwietering, M. H.; Abee, T. Air−Liquid Interface Biofilms of Bacillus Cereus: Formation, Sporulation, and Dispersion. *Appl. Environ. Microbiol.* **2007**, *73*, 1481−1488.
(36) Yap, J. X.; Leo, C. P.; Chan, D. J. C.; Mohd Yasin, N. H.; Show, P. L. Air−Liquid Interface Cultivation of Navicula Incerta Using Hollow Fiber Membranes. *Chemosphere* **2022**, *307*, No. 135625.
(37) Maleschlijski, S.; Bauer, S.; di Fino, A.; Sendra, G. H.; Clare, A. S.; Rosenhahn, A. Barnacle Cyprid Motility and Distribution in the Water Column as an Indicator of the Settlement-Inhibiting Potential of Nontoxic Antifouling Chemistries. *Biofouling* **2014**, *30*, 1055−1065.
(38) Donadt, T. B.; Yang, R. Amphiphilic Polymer Thin Films with Enhanced Resistance to Biofilm Formation at the Solid−Liquid−Air Interface. *Adv. Mater. Interfaces* **2021**, *8*, No. 2001791.
(39) Baxamusa, S. H.; Gleason, K. K. Random Copolymer Films with Molecular-Scale Compositional Heterogeneities That Interfere with Protein Adsorption. *Adv. Funct. Mater.* **2009**, *19*, 3489−3496.
(40) Woods, C. M. C.; Floerl, O.; Jones, L. Biosecurity Risks Associated with In-Water and Shore-Based Marine Vessel Hull Cleaning Operations. *Mar. Pollut. Bull.* **2012**, *64*, 1392−1401.
(41) Letcher, R. J.; Chu, S.; Smyth, S. A. Side-Chain Fluorinated Polymer Surfactants in Biosolids from Wastewater Treatment Plants. *J. Hazard. Mater.* **2020**, *388*, No. 122044.
(42) Arvaniti, O. S.; Stasinakis, A. S. Review on the Occurrence Fate and Removal of Perfluorinated Compounds during Wastewater Treatment. *Sci. Total Environ.* **2015**, *524-525*, 81−92.
(43) Gomis, M. I.; Vestergren, R.; Borg, D.; Cousins, I. T. Comparing the Toxic Potency in Vivo of Long-Chain Perfluoroalkyl Acids and Fluorinated Alternatives. *Environ. Int.* **2018**, *113*, 1−9.
(44) Lv, M.; Xie, Y.; Yu, H.; Sun, T.; Song, L.; Wang, F. Effects of Perfluoroalkyl Substances on Soil Respiration and Enzymatic Activity: Differences in Carbon Chain-Length Dependence. *J. Environ. Sci. Health, Part B* **2022**, *57*, 284−296.
(45) Liu, S.; Yang, R.; Yin, N.; Faiola, F. The Short-Chain Perfluorinated Compounds PFBS, PFHxS, PFBA and PFHxA, Disrupt Human Mesenchymal Stem Cell Self-Renewal and Adipogenic Differentiation. *J. Environ. Sci.* **2020**, *88*, 187−199.
(46) Wen, W.; Xia, X.; Zhou, D.; Wang, H.; Zhai, Y.; Lin, H.; Chen, J.; Hu, D. Bioconcentration and Tissue Distribution of Shorter and Longer Chain Perfluoroalkyl Acids (PFAAs) in Zebrafish (Danio

https://doi.org/10.1021/acssuschemeng.2c03933
ACS Sustainable Chem. Eng. XXXX, XXX, XXX−XXX

Rerio): Effects of Perfluorinated Carbon Chain Length and Zebrafish Protein Content. *Environ. Pollut.* **2019**, *249*, 277−285.
(47) Mahapatra, C. T.; Damayanti, N. P.; Guffey, S. C.; Serafin, J. S.; Irudayaraj, J.; Sepúlveda, M. S. Comparative in Vitro Toxicity Assessment of Perfluorinated Carboxylic Acids. *J. Appl. Toxicol.* **2017**, *37*, 699−708.
(48) Cheng, Y.; Khlyustova, A.; Chen, P.; Yang, R. Kinetics of All-Dry Free Radical Polymerization under Nanoconfinement. *Macromolecules* **2020**, *53*, 10699−10710.
(49) Amadei, C. A.; Yang, R.; Chiesa, M.; Gleason, K. K.; Santos, S. Revealing Amphiphilic Nanodomains of Anti-Biofouling Polymer Coatings. *ACS Appl. Mater. Interfaces* **2014**, *6*, 4705−4712.
(50) Matin, A.; Khan, Z.; Gleason, K. K.; Khaled, M.; Zaidi, S. M. J.; Khalil, A.; Moni, P.; Yang, R. Surface-Modified Reverse Osmosis Membranes Applying a Copolymer Film to Reduce Adhesion of Bacteria as a Strategy for Biofouling Control. *Sep. Purif. Technol.* **2014**, *124*, 117−123.
(51) Matin, A.; Shafi, H.; Wang, M.; Khan, Z.; Gleason, K.; Rahman, F. Reverse Osmosis Membranes Surface-Modified Using an Initiated Chemical Vapor Deposition Technique Show Resistance to Alginate Fouling under Cross-Flow Conditions: Filtration & Subsequent Characterization. *Desalination* **2016**, *379*, 108−117.
(52) Elabed, H.; Bakhrouf, A.; Hamza, R.; Azaiez, M.; Gaddour, K. Evidence of the Adaptive Response in Pseudomonas Aeruginosa to 14 Years of Incubation in Seawater. *Ann. Microbiol.* **2012**, *62*, 1385−1394.
(53) Tenhaeff, W. E.; Gleason, K. K. Initiated and Oxidative Chemical Vapor Deposition of Polymeric Thin Films: ICVD and OCVD. *Adv. Funct. Mater.* **2008**, *18*, 979−992.
(54) Şimşek, B.; Karaman, M. Initiated Chemical Vapor Deposition of Poly(Hexafluorobutyl Acrylate) Thin Films for Superhydrophobic Surface Modification of Nanostructured Textile Surfaces. *J. Coat. Technol. Res.* **2020**, *17*, 381−391.
(55) Coclite, A. M.; Lund, P.; Di Mundo, R.; Palumbo, F. Novel Hybrid Fluoro-Carboxylated Copolymers Deposited by Initiated Chemical Vapor Deposition as Protonic Membranes. *Polymer* **2013**, *54*, 24−30.
(56) Movsesian, N.; Hirth, S.; Speros, J.; Gupta, M. Robust Vapor-Deposited Antifouling Fluoropolymer Coatings for Stainless Steel Polymerization Reactor Components. *Ind. Eng. Chem. Res.* **2020**, *59*, 15264−15270.
(57) Yang, R.; Jang, H.; Stocker, R.; Gleason, K. K. Synergistic Prevention of Biofouling in Seawater Desalination by Zwitterionic Surfaces and Low-Level Chlorination. *Adv. Mater.* **2014**, *26*, 1711−1718.
(58) Shafi, H. Z.; Khan, Z.; Yang, R.; Gleason, K. K. Surface Modification of Reverse Osmosis Membranes with Zwitterionic Coating for Improved Resistance to Fouling. *Desalination* **2015**, *362*, 93−103.
(59) Huhtamäki, T.; Tian, X.; Korhonen, J. T.; Ras, R. H. A. Surface-Wetting Characterization Using Contact-Angle Measurements. *Nat. Protoc.* **2018**, *13*, 1521−1538.
(60) Spake, C. S. L.; Berns, E. M.; Sahakian, L.; Turcu, A.; Clayton, A.; Glasser, J.; Barrett, C.; Barber, D.; Antoci, V.; Born, C. T.; Garcia, D. R. In Vitro Visualization and Quantitative Characterization of Pseudomonas Aeruginosa Biofilm Growth Dynamics on Polyether Ether Ketone. *J. Orthop. Res.* **2022**, *40*, 2448−2456.
(61) Rasamiravaka, T.; Labtani, Q.; Duez, P.; el Jaziri, M. The Formation of Biofilms by Pseudomonas Aeruginosa: A Review of the Natural and Synthetic Compounds Interfering with Control Mechanisms. *BioMed Res. Int.* **2015**, *2015*, No. 759348.
(62) Cheng, Y.; Khlyustova, A.; Yang, R. All-Dry Free Radical Polymerization inside Nanopores: Ion-Milling-Enabled Coating Thickness Profiling Revealed "Necking" Phenomena. *J. Vac. Sci. Technol., A* **2022**, *40*, No. 033406.
(63) Gleason, K. K.*CVD Polymers: Fabrication of Organic Surfaces and Devices*; Wiley-VCH Verlag GmbH & Co.: Weinheim, Germany, 2015; pp 87−109.
(64) Wu, K. H.; Wang, Y. R.; Hwu, W. H. FTIR and TGA Studies of Poly(4-Vinylpyridine-Co-Divinylbenzene)− Cu(II) Complex. *Polym. Degrad. Stab.* **2003**, *79*, 195−200.
(65) Liu, A.; Goktekin, E.; Gleason, K. K. Cross-Linking and Ultrathin Grafted Gradation of Fluorinated Polymers Synthesized via Initiated Chemical Vapor Deposition to Prevent Surface Reconstruction. *Langmuir* **2014**, *30*, 14189−14194.
(66) Kelen, T.; Tudos, F. A New Improved Linear Graphical Method for Determining Copolymerization Reactivity Ratios. *React. Kinet. Catal. Lett.* **1974**, *1*, 487−492.
(67) Sheng, W.; Chen, Y.; Mao, H.; Li, Y.; Xiao, X.; Wang, C.; Ye, Y.; Liu, W. Rational Design of Vapor-Deposited Self-Crosslinking Polymer for Transparent Flexible Oxygen Barrier Coatings. *J. Appl. Polym. Sci.* **2021**, *138*, No. e50505.
(68) Tougaard, S. Accuracy of the Non-Destructive Surface Nanostructure Quantification Technique Based on Analysis of the XPS or AES Peak Shape. *Surf. Interface Anal.* **1998**, *26*, 249−269.
(69) Odian, G.. *Principles of Polymerization*; John Wiley & Sons, Inc., 2004; pp 500−507.
(70) Smolin, Y. Y.; Janakiraman, S.; Soroush, M.; Lau, K. K. S. Experimental and Theoretical Investigation of Dye Sensitized Solar Cells Integrated with Crosslinked Poly(Vinylpyrrolidone) Polymer Electrolyte Using Initiated Chemical Vapor Deposition. *Thin Solid Films* **2017**, *635*, 9−16.
(71) Semchikov, Y. D. Current Interpretation of Q-e Scheme. Review. *Polym. Sci. U.S.S.R.* **1990**, *32*, 177−187.
(72) Guo, T.-Y.; Tang, D.; Song, M.; Zhang, B. Copolymerizations of Butyl Methacrylate and Fluorinated Methacrylates via RAFT Miniemulsion Polymerization. *J. Polym. Sci.* **2007**, *45*, 5067−5075.
(73) Chen, Z. C.; Zhu, B. C.; Li, J. J.; Zhou, Y. N.; Luo, Z. H. Dual-Responsive Copolymer Poly(2,2,3,4,4,4-Hexafluorobutyl Methacrylate)-Block-Poly[2-(Dimethylamino)Ethyl Methacrylate] Synthesized via PhotoATRP for Surface with Tunable Wettability. *J. Polym. Sci., Part A: Polym. Chem.* **2016**, *54*, 3868−3877.
(74) Şimşek, B.; Karaman, M. Initiated Chemical Vapor Deposition of Poly(Hexafluorobutyl Acrylate) Thin Films for Superhydrophobic Surface Modification of Nanostructured Textile Surfaces. *J. Coat. Technol. Res.* **2020**, *17*, 381−391.
(75) Khlyustova, A.; Yang, R. Initiated Chemical Vapor Deposition Kinetics of Poly(4-Aminostyrene). *Front. Bioeng. Biotechnol.* **2021**, *9*, No. 670541.
(76) Lohse, D. J.; Hadjichristidis, N. Microphase Separation in Block Copolymers. *Curr. Opin. Colloid Interface Sci.* **1997**, *2*, 171−176.
(77) Yang, R.; Gleason, K. K. Ultrathin Antifouling Coatings with Stable Surface Zwitterionic Functionality by Initiated Chemical Vapor Deposition (ICVD). *Langmuir* **2012**, *28*, 12266−12274.
(78) Yang, R.; Asatekin, A.; Gleason, K. K. Design of Conformal, Substrate-Independent Surface Modification for Controlled Protein Adsorption by Chemical Vapor Deposition (CVD). *Soft Matter* **2012**, *8*, 31−43.
(79) Yang, R.; Goktekin, E.; Wang, M.; Gleason, K. K. Molecular Fouling Resistance of Zwitterionic and Amphiphilic Initiated Chemically Vapor-Deposited (ICVD) Thin Films. *J. Biomater. Sci., Polym. Ed.* **2014**, *25*, 1687−1702.
(80) Cheng, Y.; Feng, G.; Moraru, C. I. Micro-and Nanotopography Sensitive Bacterial Attachment Mechanisms: A Review. *Front. Microbiol.* **2019**, *10*, 191.
(81) Scardino, A. J.; Zhang, H.; Cookson, D. J.; Lamb, R. N.; de Nys, R. The Role of Nano-Roughness in Antifouling. *Biofouling* **2009**, *25*, 757−767.
(82) Carman, M. L.; Estes, T. G.; Feinberg, A. W.; Schumacher, J. F.; Wilkerson, W.; Wilson, L. H.; Callow, M. E.; Callow, J. A.; Brennan, A. B. Engineered Antifouling Microtopographies - Correlating Wettability with Cell Attachment. *Biofouling* **2006**, *22*, 11−21.
(83) Whitehead, K. A.; Colligon, J.; Verran, J. Retention of Microbial Cells in Substratum Surface Features of Micrometer and Sub-Micrometer Dimensions. *Colloids Surf., B* **2005**, *41*, 129−138.

https://doi.org/10.1021/acssuschemeng.2c03933
ACS Sustainable Chem. Eng. XXXX, XXX, XXX−XXX

(84) Bagherifard, S.; Hickey, D. J.; de Luca, A. C.; Malheiro, V. N.; Markaki, A. E.; Guagliano, M.; Webster, T. J. The Influence of Nanostructured Features on Bacterial Adhesion and Bone Cell Functions on Severely Shot Peened 316L Stainless Steel. *Biomaterials* **2015**, *73*, 185−197.
(85) Shaikh, S.; Singh, D.; Subramanian, M.; Kedia, S.; Singh, A. K.; Singh, K.; Gupta, N.; Sinha, S. Femtosecond Laser Induced Surface Modification for Prevention of Bacterial Adhesion on 45S5 Bioactive Glass. *J. Non-Cryst. Solids* **2018**, *482*, 63−72.
(86) Wassmann, T.; Kreis, S.; Behr, M.; Buergers, R. The Influence of Surface Texture and Wettability on Initial Bacterial Adhesion on Titanium and Zirconium Oxide Dental Implants. *Int. J. Implant Dent.* **2017**, *3*, 32.
(87) Flint, S. H.; Brooks, J. D.; Bremer, P. J. Properties of the Stainless Steel Substrate, Influencing the Adhesion of Thermo-Resistant Streptococci. *J. Food Eng.* **2000**, *43*, 235−242.
(88) Paxson, A. T.; Yagüe, J. L.; Gleason, K. K.; Varanasi, K. K. Stable Dropwise Condensation for Enhancing Heat Transfer via the Initiated Chemical Vapor Deposition (ICVD) of Grafted Polymer Films. *Adv. Mater.* **2014**, *26*, 418−423.
(89) Lu, A.; Gao, Y.; Jin, T.; Luo, X.; Zeng, Q.; Shang, Z. Effects of Surface Roughness and Texture on the Bacterial Adhesion on the Bearing Surface of Bio-Ceramic Joint Implants: An in Vitro Study. *Ceram. Int.* **2020**, *46*, 6550−6559.
(90) Majumdar, P.; Lee, E.; Patel, N.; Ward, K.; Stafslien, S. J.; Daniels, J.; Chisholm, B. J.; Boudjouk, P.; Callow, M. E.; Callow, J. A.; Thompson, S. E. M. Combinatorial Materials Research Applied to the Development of New Surface Coatings IX: An Investigation of Novel Antifouling/Fouling-Release Coatings Containing Quaternary Ammonium Salt Groups. *Biofouling* **2008**, *24*, 185−200.
(91) Bazaka, K.; Crawford, R. J.; Ivanova, E. P. Do Bacteria Differentiate between Degrees of Nanoscale Surface Roughness? *Biotechnol. J.* **2011**, *6*, 1103−1114.
(92) Ivanova, E. P.; Truong, V. K.; Wang, J. Y.; Bemdt, C. C.; Jones, R. T.; Yusuf, I. I.; Peake, I.; Schmidt, H. W.; Fluke, C.; Barnes, D.; Crawford, R. J. Impact of Nanoscale Roughness of Titanium Thin Film Surfaces on Bacterial Retention. *Langmuir* **2010**, *26*, 1973−1982.
(93) Braceras, I.; Pacha-Olivenza, M. A.; Calzado-Martín, A.; Multigner, M.; Vera, C.; Broncano, L. L.; Gallardo-Moreno, A. M.; González-Carrasco, J. L.; Vilaboa, N.; González-Martín, M. L. Decrease of Staphylococcal Adhesion on Surgical Stainless Steel after Si Ion Implantation. *Appl. Surf. Sci.* **2014**, *310*, 36−41.
(94) Lüdecke, C.; Bossert, J.; Roth, M.; Jandt, K. D. Physical Vapor Deposited Titanium Thin Films for Biomedical Applications: Reproducibility of Nanoscale Surface Roughness and Microbial Adhesion Properties. *Appl. Surf. Sci.* **2013**, *280*, 578−589.
(95) Mitik-Dineva, N.; Wang, J.; Truong, V. K.; Stoddart, P.; Malherbe, F.; Crawford, R. J.; Ivanova, E. P. Escherichia Coli, Pseudomonas Aeruginosa, and Staphylococcus Aureus Attachment Patterns on Glass Surfaces with Nanoscale Roughness. *Curr. Microbiol.* **2009**, *58*, 268−273.
(96) Medilanski, E.; Kaufmann, K.; Wick, L. Y.; Wanner, O.; Harms, H. Influence of the Surface Topography of Stainless Steel on Bacterial Adhesion. *Biofouling* **2002**, *18*, 193−203.
(97) Coclite, A. M.; Shi, Y.; Gleason, K. K. Super-Hydrophobic and Oloephobic Crystalline Coatings by Initiated Chemical Vapor Deposition. *Phys. Procedia* **2013**, *46*, 56−61.
(98) Çıtak, E.; İstanbullu, B.; Şakalak, H.; Gürsoy, M.; Karaman, M. All-Dry Hydrophobic Functionalization of Paper Surfaces for Efficient Transfer of CVD Graphene. *Macromol. Chem. Phys.* **2019**, *220*, No. 1900277.
(99) Coclite, A. M.; Howden, R. M.; Borrelli, D. C.; Petruczok, C. D.; Yang, R.; Yagüe, J. L.; Ugur, A.; Chen, N.; Lee, S.; Jo, W. J.; Liu, A.; Wang, X.; Gleason, K. K. 25th Anniversary Article: CVD Polymers: A New Paradigm for Surface Modification and Device Fabrication. *Adv. Mater.* **2013**, *25*, 5392−5423.
(100) Coclite, A. M.; Gleason, K. K. Global and Local Planarization of Surface Roughness by Chemical Vapor Deposition of Organosilicon Polymer for Barrier Applications. *J. Appl. Phys.* **2012**, *111*, No. 073516.
(101) Ozaydin-Ince, G.; Matin, A.; Khan, Z.; Zaidi, S. M. J.; Gleason, K. K. Surface Modification of Reverse Osmosis Desalination Membranes by Thin-Film Coatings Deposited by Initiated Chemical Vapor Deposition. *Thin Solid Films* **2013**, *539*, 181−187.
(102) Chen, Z.; Lau, K. K. S. Suppressing Crystallinity by Nanoconfining Polymers Using Initiated Chemical Vapor Deposition. *Macromolecules* **2019**, *52*, 5183−5191.
(103) Rimmer, S.; German, M. J.; Maughan, J.; Sun, Y.; Fullwood, N.; Ebdon, J.; MacNeil, S. Synthesis and Properties of Amphiphilic Networks 3: Preparation and Characterization of Block Conetworks of Poly(Butyl Methacrylate-Block-(2,3 Propandiol-1-Methacrylate-Stat-Ethandiol Dimethacrylate)). *Biomaterials* **2005**, *26*, 2219−2230.
(104) Ouhib, F.; Dirani, A.; Aqil, A.; Glinel, K.; Nysten, B.; Jonas, A. M.; Jerôme, C.; Detrembleur, C. Transparent Superhydrophobic Coatings from Amphiphilic-Fluorinated Block Copolymers Synthesized by Aqueous Polymerization-Induced Self-Assembly. *Polym. Chem.* **2016**, *7*, 3998−4003.
(105) Leonardi, A. K.; Ober, C. K. Polymer-Based Marine Antifouling and Fouling Release Surfaces: Strategies for Synthesis and Modification. *Annu. Rev. Chem. Biomol. Eng.* **2019**, *10*, 241−264.
(106) Klockgether, J.; Munder, A.; Neugebauer, J.; Davenport, C. F.; Stanke, F.; Larbig, K. D.; Heeb, S.; Schöck, U.; Pohl, T. M.; Wiehlmann, L.; Tümmler, B. Genome Diversity of Pseudomonas Aeruginosa PAO1 Laboratory Strains. *J. Bacteriol.* **2010**, *192*, 1113−1121.
(107) Graham, M.; Mosier, A. P.; Kiehl, T. R.; Kaloyeros, A. E.; Cady, N. C. Development of Antifouling Surfaces to Reduce Bacterial Attachment. *Soft Matter* **2013**, *9*, 6235−6244.
(108) Maggay, I. V.; Suba, M. C. A. M.; Aini, H. N.; Wu, C. J.; Tang, S. H.; Aquino, R. B.; Chang, Y.; Venault, A. Thermostable Antifouling Zwitterionic Vapor-Induced Phase Separation Membranes. *J. Membr. Sci.* **2021**, *627*, No. 119227.
(109) Dong, Z.; Lu, J.; Wu, Y.; Meng, M.; Yu, C.; Sun, C.; Chen, M.; Da, Z.; Yan, Y. Antifouling Molecularly Imprinted Membranes for Pretreatment of Milk Samples: Selective Separation and Detection of Lincomycin. *Food Chem.* **2020**, *333*, No. 127477.
(110) Venault, A.; Lai, M. W.; Jhong, J. F.; Yeh, C. C.; Yeh, L. C.; Chang, Y. Superior Bioinert Capability of Zwitterionic Poly(4-Vinylpyridine Propylsulfobetaine) Withstanding Clinical Sterilization for Extended Medical Applications. *ACS Appl. Mater. Interfaces* **2018**, *10*, 17771−17783.
(111) Gu, Q.; Jia, Z.; Zhen, T. Preparation of Quaternized Poly(Vinylidene Fluoride) Membrane by Surface Photografting and Its Antifouling Performance for Alkaline Proteins. *Desalination* **2013**, *317*, 175−183.
(112) Wang, Z.; Cousins, I. T.; Scheringer, M.; Hungerbuehler, K. Hazard Assessment of Fluorinated Alternatives to Long-Chain Perfluoroalkyl Acids (PFAAs) and Their Precursors: Status Quo, Ongoing Challenges and Possible Solutions. *Environ. Int.* **2015**, *75*, 172−179.
(113) Piola, R. F.; Dafforn, K. A.; Johnston, E. L. The Influence of Antifouling Practices on Marine Invasions. *Biofouling* **2009**, *25*, 633−644.

https://doi.org/10.1021/acssuschemeng.2c03933
ACS Sustainable Chem. Eng. XXXX, XXX, XXX−XXX